Hydrogeology Journal (2021) 29:2245–2266
https://doi.org/10.1007/s10040-021-02343-x

REPORT

Hydrochemistry and environmental isotopes of spring water and their relation to structure and lithology identified with remote sensing methods in Wadi Araba, Egypt

Manal Wannous[1] · Barbara Theilen-Willige[2] · Uwe Troeger[1,2] · Marianne Falk[3] · Christian Siebert[4] · Florian Bauer[5]

Received: 6 July 2020 / Accepted: 24 March 2021 / Published online: 4 June 2021

Abstract

Springs located at the historical sites of Wadi Araba (Eastern Desert of Egypt) and emerging from the escarpments of the Northern and Southern Galala Plateaus were investigated. A combination of methods, including hydrochemistry, stable and radioisotope composition, and structural analyses based on satellite data, provided information about the structure of the subsurface and the derived groundwater flow paths. Satellite images reveal karst features within the northern plateau, e.g. conical landforms. Karstic caves were documented along both escarpments. Chemical analysis of floodwater from Wadi Araba indicates higher concentrations of terrestrial salts compared to floodwaters from central and southern parts of the desert. $\delta^{18}O$ and $\delta^{2}H$ signatures in spring waters resemble those of floodwater and fall on the global meteoric water line, confirming their fast infiltration with minor influence of evaporation. The aquifer feeding the springs of the Northern Galala Plateau has low retention and the springs dry out quickly, even after heavy rainfall. Contrastingly, ^{3}H activities in springs emerging from the Southern Galala Plateau refer to much slower subsurface passage. With respect to ^{3}H content (3.8 TU) in recent flood waters, the spring water at Southern Galala Plateau contains about 40% recently recharged groundwater. However, its largest spring—the St. Antony spring—discharges water with a radiocarbon age of about 15,000 years. In combination with this spring's constant and high discharge over a period of several months, that age estimate suggests a large reservoir with moderate to high retention.

Keywords Groundwater recharge · Egypt · Stable isotopes · Mean residence time · Lineaments

Introduction

In the Eastern Desert of Egypt, as in most arid regions worldwide, groundwater is the only noteworthy source for water supply. Since ancient times, the establishment of settlements and agricultural areas has relied on that source, particularly on perennial discharging springs. That situation is observable in Wadi Araba, a 110-km long and about 20-km wide arcuate valley, which is flanked by the Northern and Southern Galala Plateaus, and finally opens into the Gulf of Suez in the northwestern part of the Red Sea (Fig. 1). In the Wadi Araba Valley, groundwater is abstracted from springs and wells scattered over a wide area (Fig. 2). The springs predominantly originate from the fractured aquifer forming the Galala Plateaus (El-Sadek et al. 1998).

The northern part, which extends up to the Suez Governate, contains several thermal springs. Previous studies investigated their stable isotope composition, mineralization, the source of the enhanced temperatures and energy potential (Sturchio et al. 1996; Abouzied et al. 2020). Nassim (1990) applied aerial images to analyse lineaments that focus the surface water drainage, mapped springs in the region, and classified

✉ Manal Wannous
manal.wannous@tu-berlin.de

[1] Water Engineering Department, Central Institute El Gouna, Technische Universität Berlin, Acker Str.76, 13355 Berlin, Germany

[2] Institute of Applied Geoscience, Technische Universität Berlin, Ernst-Reuter-Platz 1, 10587 Berlin, Germany

[3] Museum of Natural History, Leibniz Institute for Evolution and Biodiversity Science, Invaliden Str. 43, 10115 Berlin, Germany

[4] Department of Catchment Hydrology, Helmholtz Centre for Environmental Research – UFZ, Theodor-Lieser Str. 4, 06120 Halle, Germany

[5] Karlsruher Institute of Technology Campus Nord, Hermann-von-Helmholtz-Platz 1, 76344 Eggenstein-Leopoldshafen, Karlsruhe, Germany

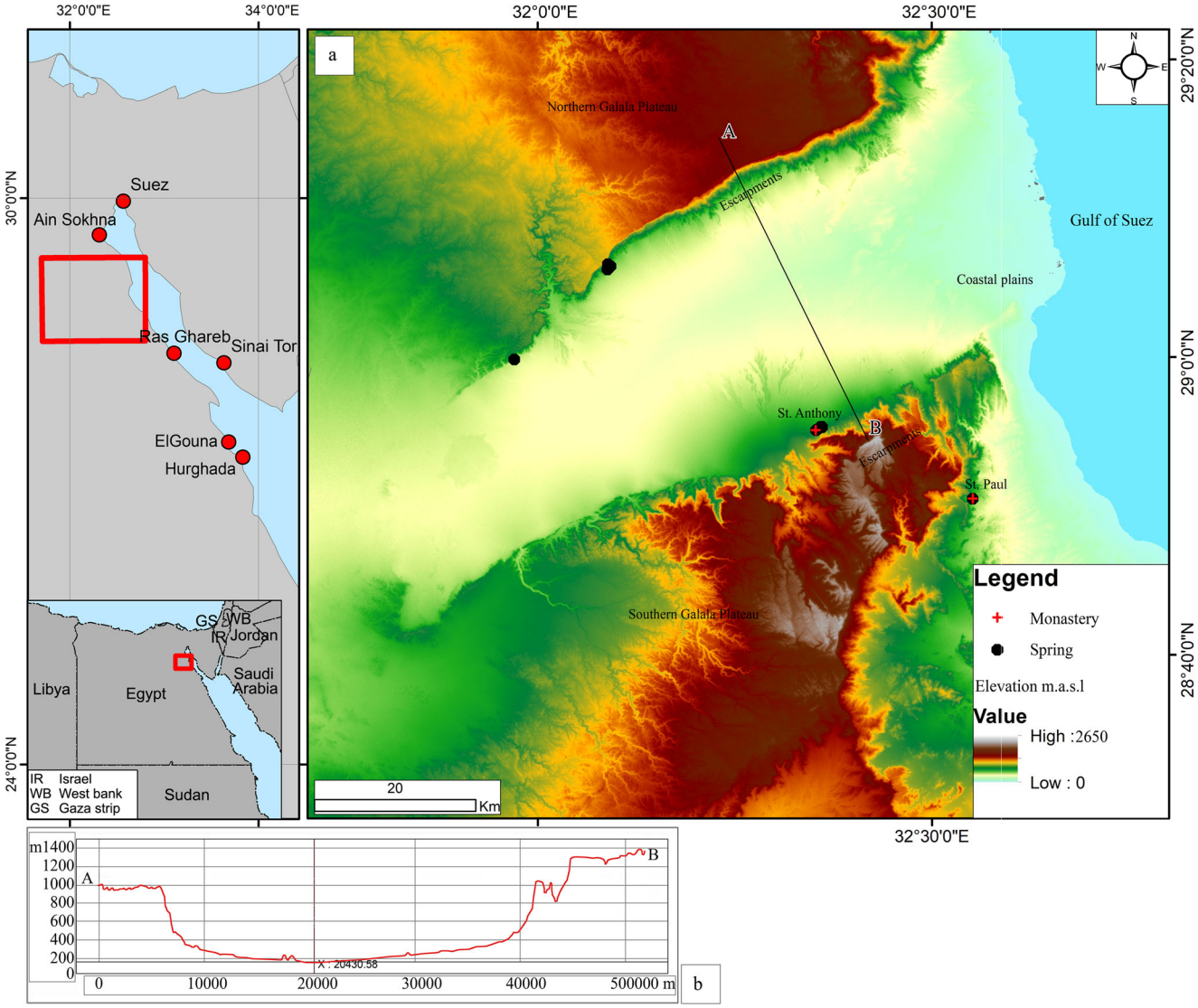

Fig. 1 **a** Map indicating the location and morphology of Wadi Araba, which opens into the Gulf of Suez at the north-western end of the Red Sea. **b** Topographic cross section perpendicular to the valley axis. Episodic floods formed erosional fluvial landforms including large dry beds and a meandering bed in the central part of Wadi Araba

groundwater aquifers in Wadi Araba. Following local knowledge, a number of springs has been documented along the northern flank of Wadi Araba, usually flowing in small ponds used by small communities.

Particularly in the Southern Galala Plateau region, productive springs have been used since ancient times to provide water for settlements such as the two >1,500-year-old monasteries—St. Anthony's Monastery (SAM), located at the southern flank of Wadi Araba, and St. Paul's Monastery (SPM), located some 20 km further SE (Fig. 1). Within the area of SAM several springs emerge along an 800-m-long lineament and are intended as emergency source of water supply for 350 residents and for irrigation purposes. Unlike SAM, in the area of SPM a single spring emerges, intended to serve the same purpose.

Except for a few quality data of the main springs of St. Anthony and St. Paul (Nassim 1990), neither recharge mechanisms nor discharge dynamics of the springs that emerge in Wadi Araba and in these historical sites have been adequately investigated yet. According to the authors' own measurements, the largest of the SAM springs yields an average discharge of 87 m^3/day and is flowing all year round, while many of the small springs along the northern rim of the valley fall dry. Thus, this study aims at mapping and characterizing the groundwater springs in Wadi Araba, with a special emphasis on the springs at SAM and SPM. The evaluation of satellite image data can contribute to: (1) the detection of fault and fracture zones influencing the groundwater flow and fluid permeability of rocks, (2)

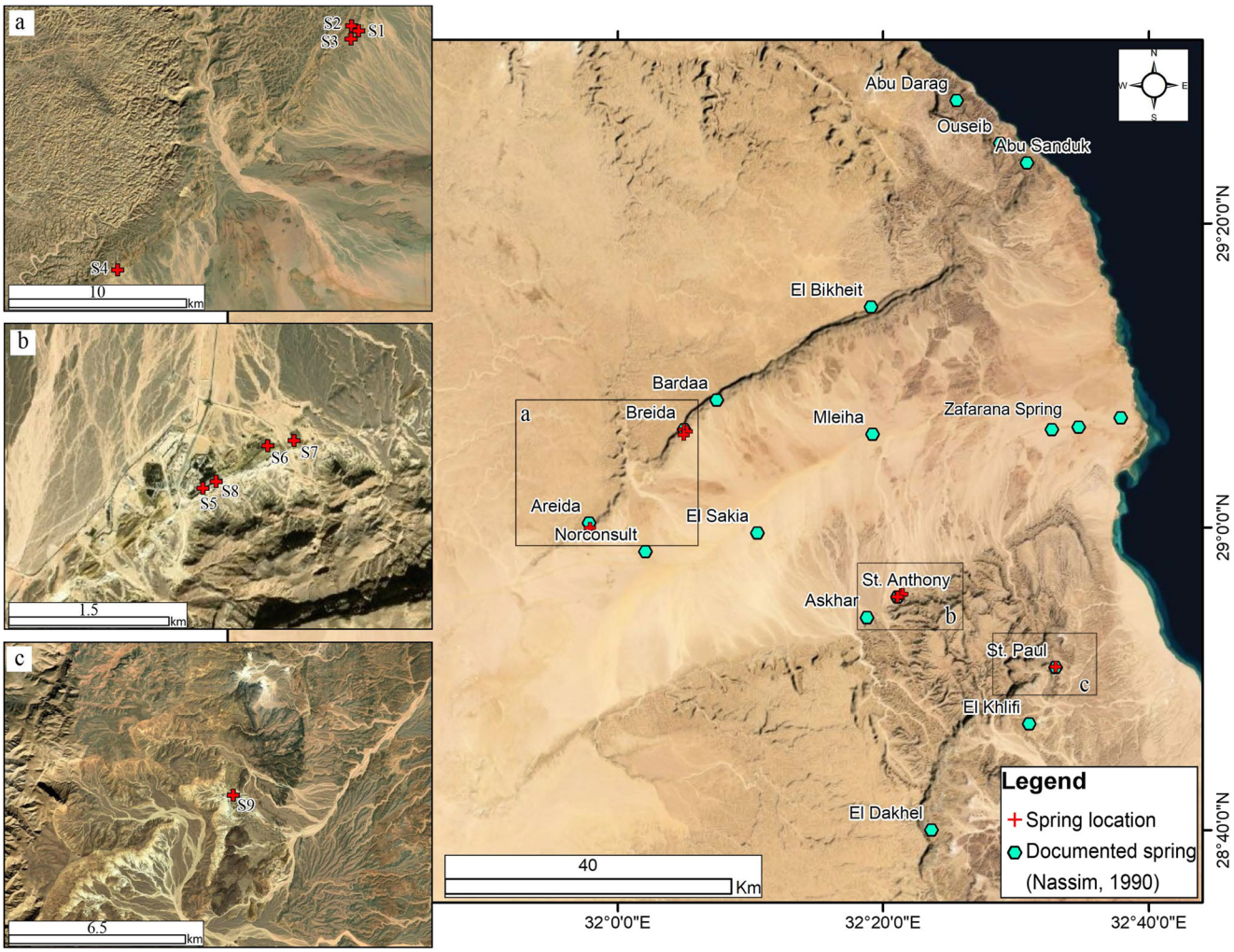

Fig. 2 Map indicating the locations of sampling points in the Wadi Araba area. Inset maps focus on the: **a** spring group along the northern rim of the Wadi; **b** the Monastery of St. Anthony at the southern rim; **c** the Monastery of St. Paul, outside the Wadi on the Southern Galala Plateau

deriving the youngest fault pattern cutting the most recent sediments as preferable infiltration pathways, (3) mapping of structural features and lithologic units which play a role in storing and transporting groundwater, and (4) monitoring of morpho-dynamic processes influencing the infiltration of surface water such as sediment flow, accumulation and erosion.

The chemical analyses of water samples from spring locations detected in the area clarify which kind of aquifer is discharging to these springs and what kind of water/rock interactions take place in the subsurface. The stable isotope signatures of ^{18}O and ^{2}H contribute to the understanding of (1) climate conditions at which the water was recharged and (2) whether their isotope signatures indicate contributions of groundwater from the Nubian Sandstone aquifer, which springs elsewhere in the region. The radio isotope analyses of ^{3}H and ^{14}C were used to calculate the mean resident time of groundwater in the aquifer, which also allows insight into whether or not the emerging groundwaters are at least partially recharged recently by occasional rainfall or flash floods.

Study area

Climate

The climate in the Eastern Desert of Egypt is arid and generally characterized by hot summers and moderate winters. Sporadic and short precipitation events take place in winter months (between October and April) and their spatial extension and intensity are extremely variable, e.g. the event on 27 October 2016 produced more than 100 mm of precipitation and caused a destructive flash flood in the town of Ras Ghareb (Saber et al. 2020), while north (Suez) and central (El Gouna) (Fig. 1), less than 20 mm of precipitation occurred.

The orographic influence of the Galala Plateaus on cloud distribution in Wadi Araba may lead to rain-bearing cloud concentration above the Northern and Southern Galala Plateaus. Observations in Suez, which has the closest climate station to Wadi Araba, show erratic precipitation events with usually low amounts, less than 6 mm/day, while only a few events produced more than 10 mm/day (Fig. 3).

The climate data presented in Fig. 4 were obtained from El Gouna climate station, situated at the Red Sea coastal plain (27.43 E, 33.66 N). The monthly averages and standard deviations are calculated using the data measured in the period between March 2014 and January 2019 with a time interval of 10 min. The range between average ± standard deviation represents 68% of the data.

The highest temperatures are recorded between June and August (>30 °C) and the lowest in December/January (<20 °C). The relative humidity with an annual average of 47% shows a weak seasonal variation with a minimum between May and August (average 45%) and a maximum between October and December (average of 50%). Evaporation data from the region were reported by Awad et al. (1996) with a maximum annual mean value in June with 10.11 mm/day and a minimum in December with 6.11 mm/day.

Geomorphology

The geomorphological units of the landscape that are important for recharge and precipitation runoff can be differentiated. The Northern Galala Plateau shows typical conical landforms related to weathering of limestones and dolomites during more humid conditions in the past. The uncovered, flat, exposed fractured carbonate rocks show good properties for recharge.

The Southern Galala Plateau is block-wise intersected by distinct visible escarpments related to fault zones (Fig. 1). This area shows traces of an intense erosion such as deeply incised valleys. Sand and gravel sediments are accumulated in small depressions. While the northern escarpment is forming an almost continuous line, the southern border of the Wadi Araba basin is characterized by dissected front lines, intersected by larger N–S-oriented valleys. Along the northern escarpments, block gliding and rockfall towards the southern direction are a common feature. This morphology enables recharge in the hollows and fissures left behind and the steep slopes promote more surface runoff. The drainage network indicates a relatively flat bedding of the rocks and is probably the result of parallel tectonic structures.

The interaction between fluvial and tectonic processes is evident as the development of channels is influenced by subsurface structures and geotectonic movements related to plate tectonic rifting activity in the Gulf of Suez area and northward movements of the African Plate.

Geology and tectonic

Wadi Araba is a structurally controlled tectonic basin (Fig. 5). The major force of the structural development in this area was

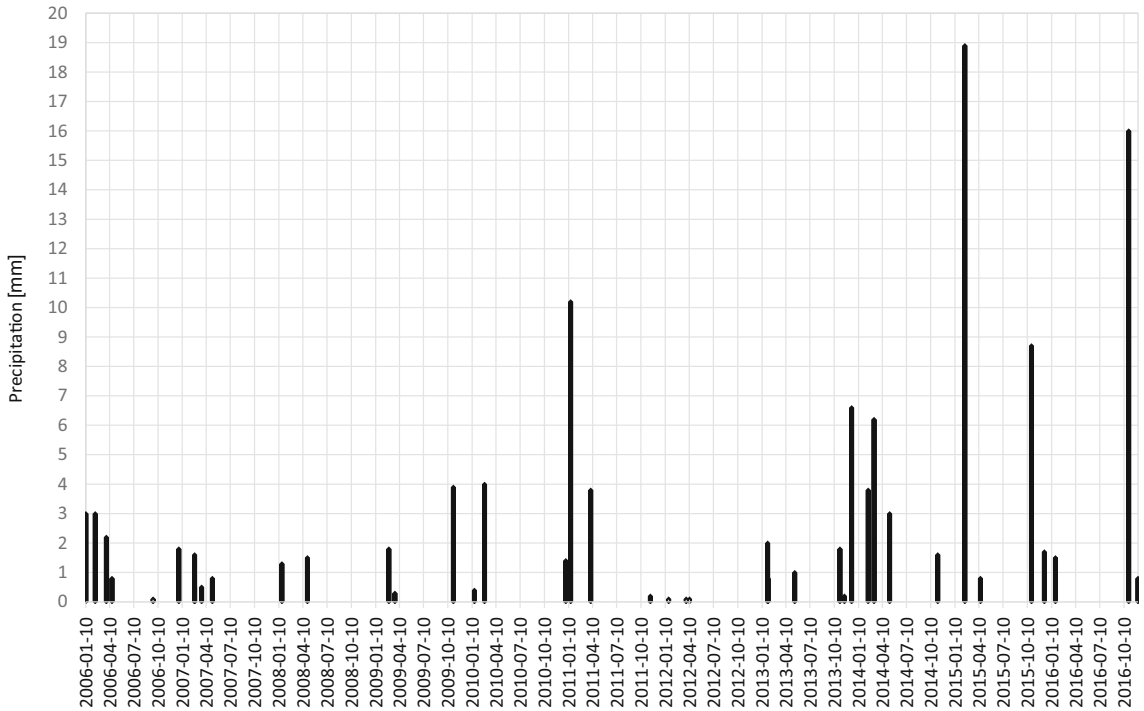

Fig. 3 Precipitation depth for the period Jan 2006 to Dec 2016 at Suez climate station (source: National Water Research Center (Egypt), Rainfall data of the Suez climate station, obtained through personal communications, 2020)

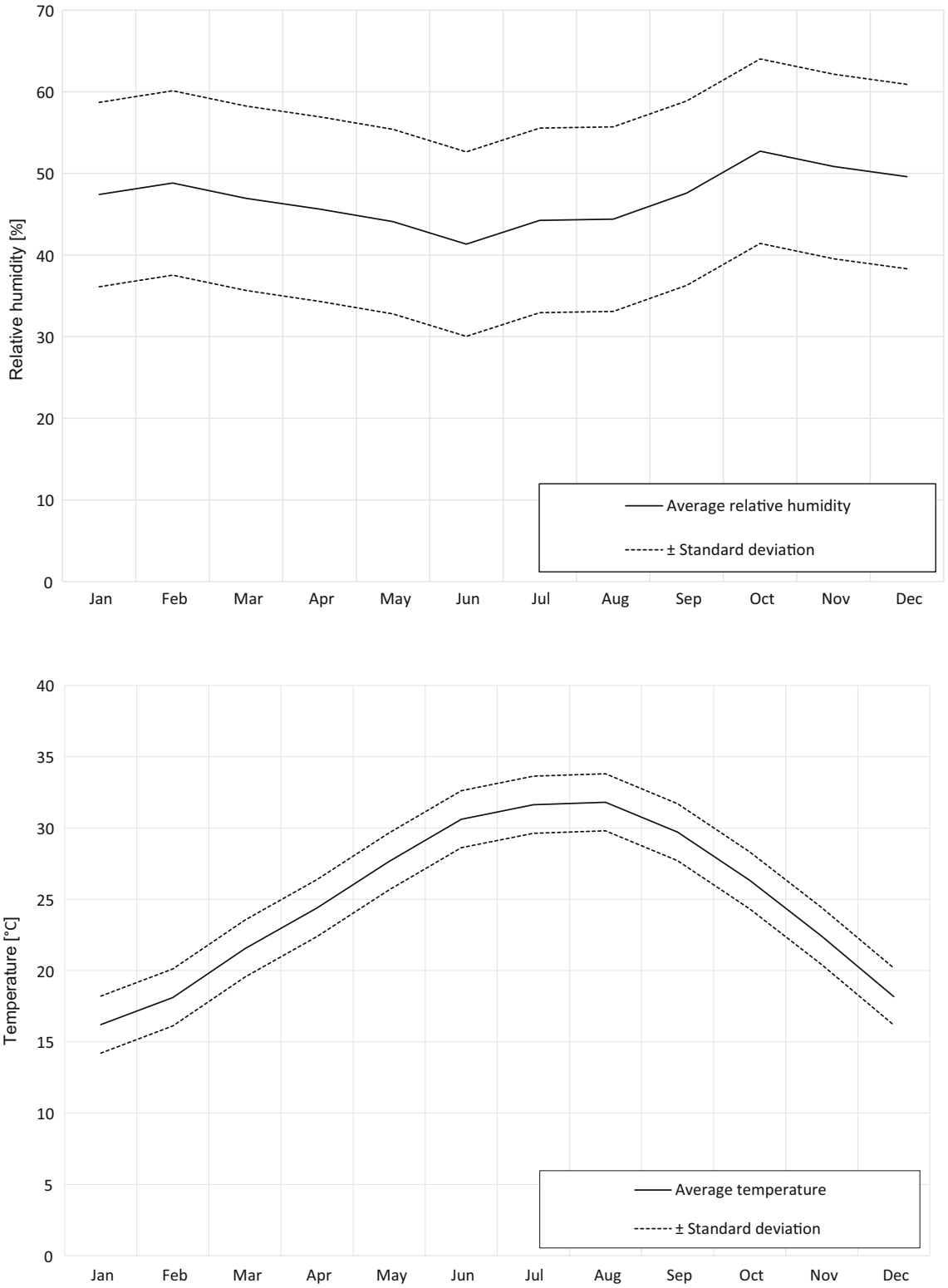

Fig. 4 Air temperature and relative humidity records at El Gouna climate station (based on 10 min time series data)

the opening processes of the Red Sea, which started in the Miocene and continues today (Bosworth and Durocher 2017). The stratigraphy is divided into three major units, which are related to the evolution of the Red Sea/Gulf of Suez, i.e. the pre-rift (Pre-Oligocene), syn-rift units (Late Oligocene–Middle Miocene) and post-rift units (Late

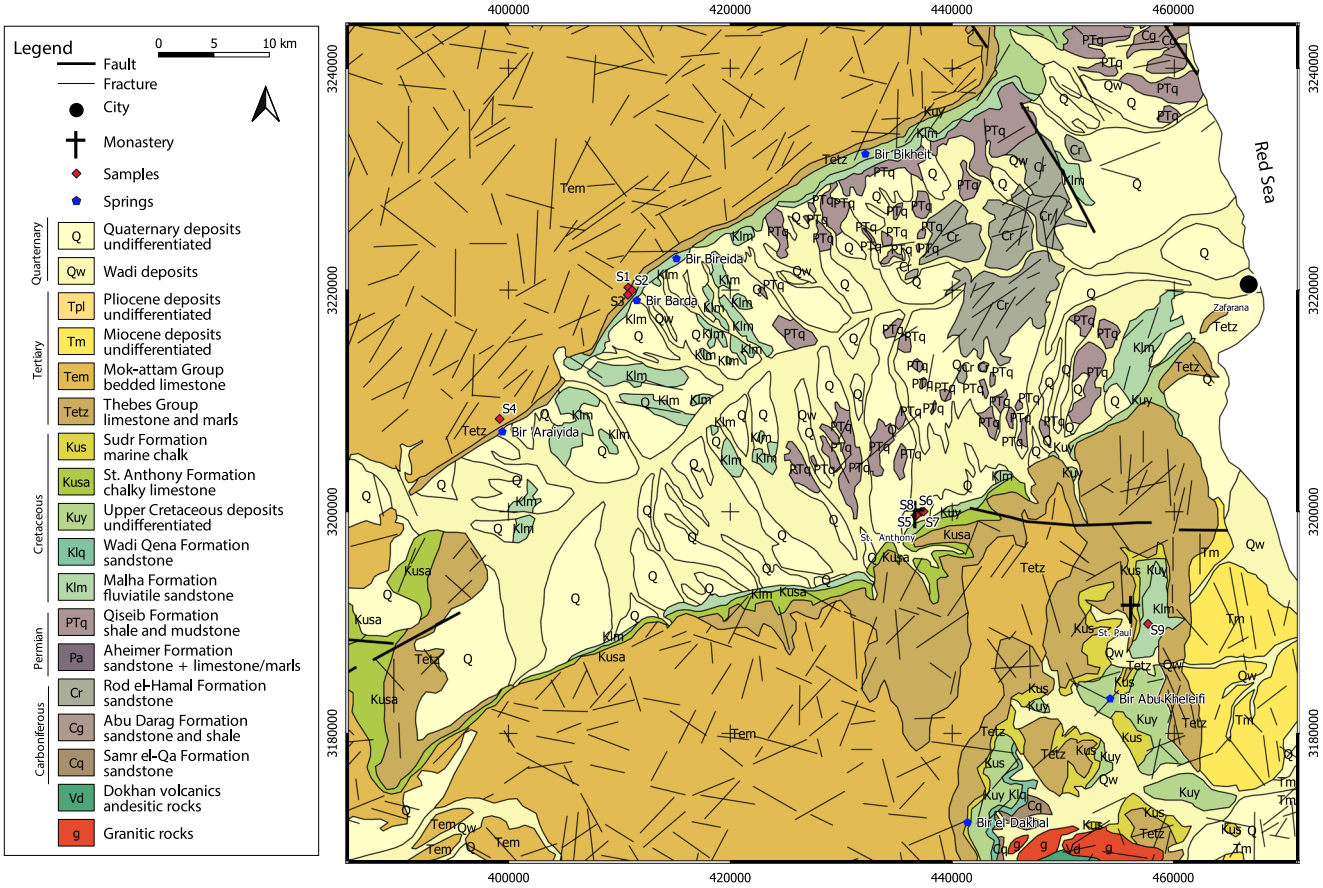

Fig. 5 Geologic map of Wadi Araba with the locations of St Anthony's Monastery (SAM) and St Paul's Monastery (SPM); modified after Klitzsch et al. (1987)

Miocene/Pliocene to Quaternary; Klitzsch and Linke 1983; Alsharhan 2003; Fig. 6).

The Nubian Sandstone Aquifer System (NSAS) in the study area overlies the metamorphic basement (Fig. 7) and contains formations from Paleozoic to Mesozoic age: the Lower Cretaceous Malha Fm. (Nubia A), the Lower Carboniferous Abu Durba Fm. (Nubia B) and the even older Nubia Fm. (C + D).

As a result of the regional compressional and extensional forces, along the Gulf of Suez (El-Naby et al. 2009), a complex structural system of numerous horsts and grabens with variable relief and dimensions developed (El-Naby et al. 2010). Over the entire region, the three major tectono-sedimentary features, i.e. Wadi Araba and the flanking Northern and Southern Galala Plateaus, are dissected by a complex pattern of NW–SE, N–S, and E–W directed faults. Both Plateaus consist of clastic sedimentary rocks of Late Paleozoic to Early Cretaceous age, and carbonatic strata of Cretaceous to Paleogene age (Kuss et al. 2000; El-Sadek 2009). The trend of the deep fault pattern, which affects the basement, the overlying Mesozoic, and recent sediments, oscillates around the E–W direction (El-Sadek 1998), and these fault patterns are assumed to be linked at depth with the NW–SE faults in northern Egypt (Abdel-Fattah et al. 2013).

At depth, in the study area, two almost parallel basic to ultrabasic dykes exist, which divide it into two parts: an eastern shallow part and a western deep one (El-Sadek 2009). Moreover, the study area represents a series of horsts (domes or anticlines) and grabens (troughs, basins or synclines). A meridional cutting geological profile is based on a cross section provided by Höntzsch et al. (2011) and preceding works (Moustafa and El-Rey 1993; Schütz 1994; Moustafa and Khalil 1995; Scheibner et al. 2001; Fig. 7).

Hydrogeology

Along the Gulf of Suez, groundwater emerges in the form of springs and artesian wells from the Nubian Sandstone aquifer; this was recharged in the late Pleistocene (Gat and Isaar 1974; Sturchio et al. 1996). Abouzied et al. (2020) reported that flash flood events contribute to the recharge of groundwater in the Eastern Desert along the Gulf of Suez; however, these assumptions are yet to be proven by calibrated infiltration models or age determination.

Period	Epoch	Symbol	Geological unit	Hydrogeology/Lithology
Quaternary		Q; Qw	undifferentiated	Predominantly fluvial deposits (fan, wadi)
Tertiary	Miocene	Tm	undifferentiated	
	Oligocene	To	undifferentiated	Gravel and sands,
	Eocene (middle)	Tem	Mokattam Grp.	Shallow marine, dense and imbedded limestone
	Eocene (lower)	Tetz	Thebes Grp. and Abu Rimth Fm.	Imbedded limestones and marl, clasts of reefal limestone and other shallow carbonates
Cretaceous	Mastrichian		Sudr Fm.	Limestone
		Categorised under Kuya	Maghra El-Bahari Fm	
	Campanian	Kusa	St. Anthony Fm.	Sequence of chalky to sandy limestone and marls
		Categorised under Kuya	Adabia Fm	
	Santon/Coniac		Matulla	Sandstone with intercalated shales
	Turonian	Kug	Wata/Galala Fm.	Dolostone/limestone intercalated by shale at its lower part
		Categorised under Kuya	Maghra El-Hadida Turonian	
	Cenomanian		Raha	Shales, lower part sandstone with dolostone beds
		Kuyb	Galala, Om Omaeiyid Hawashiya and Rakhiat Fms	
	Lower Cretaceous	Klm	**Malha Fm.**	Fluviatile sandstone, with conglomerates (Nubia A)
Permo-Triassic	Permo-Triassic	PTq	Qisieb Fm.	Red shale, mud- and sandstone
Carboniferous	Upper Carbon.	Cr	Rod El-Hamel Fm.	Sandstone
		Cg	Abu Darag Fm.	Dark sandstone and shale altering with fossiliferous limestone
	Lower Carbon.		**Abu Durba**	Sandstone (Nubia B)

Fig. 6 Stratigraphy of the geological units, exposed in the area of Wadi Araba. Geological units that belong to the Nubian Sandstone Aquifer System (NSAS) are given in bold, productive aquifers are indicated by blue background

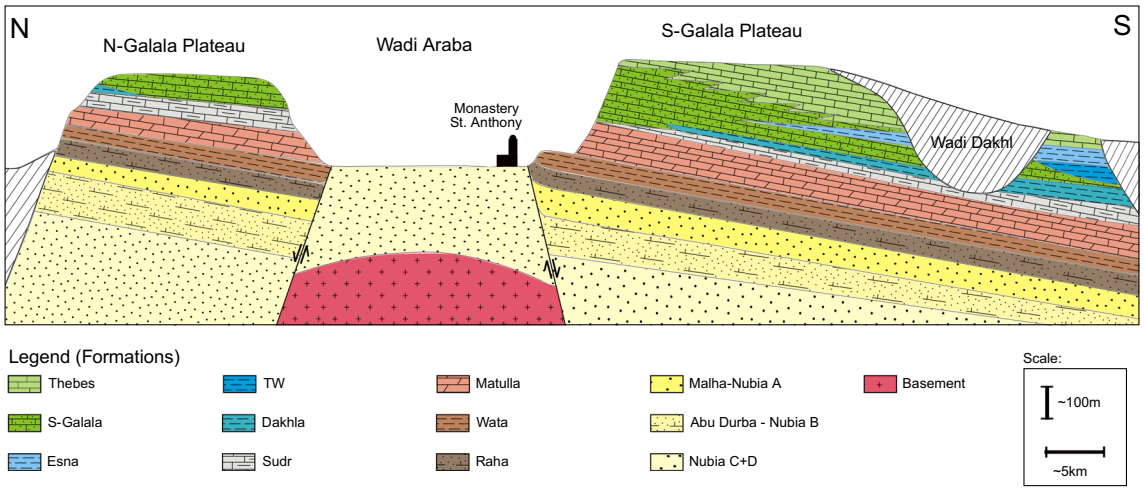

Fig. 7 Stratigraphic cross section through Wadi Araba, crossing the area of SAM. Modified after Höntzsch et al. (2011)

Table 1 Chemical and stable isotopes analysis results in the nine sampled springs in the Wadi Araba area, (−) = not determined

Site ID	Local name	X (UTM)	Y (UTM)	Sampling date	TDS [mg/L]	T [°C]	EC [mS/cm]	pH	Cl [mg/L]	NO_3	SO_4	HCO_3	Br	F	Ca	Mg	Na	K	$\delta^{18}O$ [‰ SMOW]	$\delta^{2}H$	^{3}H TU
Groundwater samples																					
S1	Not specified	410812	3220212	30.05.2018	1,629	28.3	2.4	7.3	521	3.5	319	264	0.4	0.8	109	79.6	314	8.31	−6.7	−43.1	–
S2	Not specified	411156	3219963	30.05.2018	2,249	24.1	5.3	7.1	730	25.8	432	307	0.6	1.3	159	105	464	12.6	−6.9	−42.4	–
S3	Not specified	410774	3219565	30.05.2018	1,756	27.6	2.8	6.9	525	2.7	346	305	0.3	0.9	143	88.7	322	20.9	−6.8	−42.3	–
S4	Not specified	399214	3208365	30.05.2018	1,797	28.2	2.8	7.5	605	2.8	200	405	0.3	1.02	118	85.2	351	12.2	−5.2	−31.8	–
S5	St. Anthony spring	436680	3199634	01.10.2016	1,370	–	2.1	8.1	441	0.4	358	299	0.1	0.1	124	52.8	255	4.3	−5.9	−39.1	–
S5	St. Anthony spring	436680	3199634	27.02.2018	1,465	24.0	2.1	7.3	407	1.1	314	279	0	0	140	57.1	246	4.8	−6.4	−37.2	<0.3
S6	Ain Smar	437213	3199976	27.02.2018	2,604	20.7	3.7	8.5	700	0.9	747	283	0.3	0	91	44	715	9.9	−7.3	−46.7	1.1
S7	Agathon spring	437430	3200017	27.02.2018	2,548	21.1	3.5	7.8	657	0.7	776	275	0.3	0	130	54.1	628	14	−7.6	−49.7	1.5
S8	Ain Aladra	436788	3199687	27.02.2018	1,547	17.7	2.2	7.8	437	0.6	349	255	0.3	0	141	58.8	281	9.1	−6.2	−37.6	< 0.6
S9	St. Paul spring	457652	3189870	27.02.2018	2,172	19.5	2.9	8.5	616	17.2	466	370	0.2	0	164	58.5	454	10.4	−5.9	−37.1	1.1
Rainwater samples																					
R1	Hurghada-ElGouna	535705	3019469	03.03.2014	–	–	–	–	26.2	30	16.6	–	–	0.9	41.6	3.3	11.6	3.2	–	–	–
R2	Hurghada-ElGouna	541232	3010748	09.03.2014	–	–	–	–	6.3	0.9	2.6	–	0.4	0.6	7.1	0.1	–	0.3	–	–	–
R3	Hurghada-ElGouna	535705	3019469	09.03.2014	–	–	–	–	8.8	0.5	4.8	–	0.4	0.7	17.9	1.4	–	0.6	–	–	–
R4	Hurghada-ElGouna	566112	3030731	27.10.2016	–	25.1	0.4	6.5	54	12.3	43.9	17.4	0.1	0	31.5	3.1	21.2	0.9	–	–	–
R5	ElGouna	566749	3031656	23.02.2018	–	–	–	–	19.7	0	25.5	–	0.1	0	28.4	2.6	14	4.4	3.7	22.0	–
Flood water samples																					
F1	St. Anthony	437557	3200053	18.02.2019	2,680	–	3.5	7.7	695	17.7	799	192	0.4	0	358	33.3	415	18.8	0.7	14	3.8
F2	Hurghada-ElGouna	566819	3030495	28.10.2016	492	25.3	0.6	7.8	61.4	12.7	159	91.5	0.02	0.2	79.6	7.7	93.3	14.8	–	–	–
F3	Hurghada-ElGouna	563710	3029094	29.10.2016	903	25.9	1.2	7.8	175	1.9	278	78.4	0.2	0.3	147	14	130	11.6	–	–	–
F4	Hurghada-ElGouna	563710	3029094	03.11.2016	952	22.8	1.2	8.2	184	18	369	91.5	0.1	0	148	14.9	98.2	13.8	–	–	–
F5	El Quseir	–	–	–	150	–	–	–	–	–	–	–	–	–	–	–	–	–	−0.8	1.9	–

In the study area, four major aquifers exist: (1) Quaternary aquifer, (2) Upper Cretaceous aquifer, (3) Lower Cretaceous aquifer and (4) the Carboniferous aquifer (Nassim 1990; Fig. 6). The Quaternary aquifer occurs along the major dry Wadi and gets recharged during the rare occasional rainfall events. Three wells with yield between 5 and 23 $m^{3/}$day and one spring in the east of the study area derive water from that aquifer (Nassim 1990; Fig. 2).

The Upper Cretaceous aquifer (the formations of Wata, Raha, Matulla) hosts groundwater with total dissolved solids (TDS) of 1,200–8,000 ppm (Nassim 1990). The most productive aquifer is the Lower Cretaceous, which is known as the Nubian Sandstone, mainly recharged during pluvial times (Abdel Moneim 2005). This aquifer is composed of coarse sandstone and sands and has confined conditions in the central area of the case study. The groundwater in this aquifer is brackish with salinities of 1,000–2,600 ppm (Nassim 1990). The Carboniferous aquifer is mainly composed of sand and sandstone interlaced with clay layers that create confining conditions in the Zafarana area in the east. One disappeared spring, Abu Darag (Fig. 2), can be associated to that aquifer and discharged water with TDS of 2300 ppm.

Local nomads living in the area reported 30 groundwater emergences, of which 17 are springs and 13 locations are shallow hand dug wells or drilled wells that reach 86–1,200 m depth (Nassim 1990). Out of the 17 springs, 13 discharge from the Upper Cretaceous aquifer with average rates of 2.5 m^3/day during summer and 5 m^3/day during winter time, respectively (Nassim 1990).

The springs emerge at different elevations and from different stratigraphic units indicating that groundwater occurrence is not only influenced by lithologic properties, but also by the position and hydraulic properties of fractures and fault zones. Due to the still active neotectonic activities, faults and fractures have developed recently and play an important role in conduit development. In addition, karstification of the fractured limestones of the Galala led to the formation of cavities and a stochastic drainage system in the plateaus, hampering the exact determination of spring catchments.

Materials and methods

The interdisciplinary approach used in the scope of this study comprises hydrological field investigations, evaluation of remote sensing data, and geological, geomorphological and topographic data.

Water samples and analyses

Two rainwater samples were collected in the area of Hurghada in 2016 (R4) and 2018 (R5) to analyse major ion composition in rainfall. Both were supplemented by data from Askar (2014) and Hadidi (2016) for precipitation (R1, R2, R3). In the period between 2016 and 2019 water samples from 9 springs in the area of Wadi Araba were collected for chemical composition, stable isotopes and ^{3}H analysis (Table 1; Fig. 2). In addition to these samples, a floodwater sample was collected on 18 February 2019, 3 days after a rainfall event (≈3 mm event at El Gouna weather station), directly from the area of SAM, to analyse the ^{3}H content and stable isotopes in the provoking rainfall. The main spring at SAM was sampled for ^{14}C analysis to determine the groundwater residence time.

The field parameters temperature (T), pH, and electrical conductivity (EC) were measured at each location using WTW portable devices. Alkalinity was determined using gran titration. To analyse anions and cations in flood water and groundwater, samples were filtered in the field using a 0.45-μm filter and filled into 50-ml bottles. The cation samples were acidified by adding 0.2 ml of HNO_3 and all samples were treated with 0.2 ml of $C_4H_8N_2S$, respectively. Major anions (NO_3, SO_4, Cl, Br) were analysed using a Metrohm 881 Compact Ion Chromatograph pro Anion–MCS. Major cations (Ca, Mg, Na, K) were analysed using an Agilent 715 ICP-OES. All analyses were performed in a laboratory of the Technical University of Berlin at the El Gouna Campus, Egypt.

Samples for stable isotopes of water were filtered into 2-ml bottles, finally sealed to prevent evaporation according to IAEA (2009) and later measured with a PICARRO L1102-i isotope analyser at Museum of Natural History in Berlin (Germany). The L1102-i is based on the WS-CRDS (wavelength-scanned cavity ring down spectroscopy) technique (Gupta et al. 2009).

The stable isotope ratios are expressed in the conventional delta notation (δ^{18}O, δD) in permil (‰) versus Vienna Standard Mean Ocean Water (VSMOW). For each sample, six replicate injections were performed and arithmetic average and standard deviations (1 sigma) calculated. The reproducibility of replicate measurements is generally better than 0.1‰ for oxygen and 0.5‰ for hydrogen.

To determine the ^{3}H content in the water, 1,000 ml could be sampled in the southern escarpment, from springs S5–S9 only (Fig. 2). Tritium analyses were carried out by applying the electrolytic enrichment using Liquid Scintillation Counting (LSC) in the Hydroisotop Laboratory, Schweitenkirchen (Germany) with a detection limit of 0.5 TU. Values are reported in tritium units (TU) where 1 TU equals an activity of 0.119 Bq/L (IAEA 1992). The tritium half-life time is (4,500 ± 8) days (≈12.3 years; Lucas and Unterweger 2000).

To estimate the groundwater age of the recent water, ^{3}H input function of the sampled water must be reconstructed for several periods in the past using the tritium values for the rainfall in the country (if available) or neighbouring regions (IAEA 1990; Geyh et al. 1995).

Following Małoszewski and Zuber (1982), the mathematical form to describe the input-output concentration of the tracer under steady state flow condition is given by Eq. (1):

$$C_{\text{out}}(t) = \sum_{\tau=0}^{\infty} C_{\text{in}}(t-\tau) \cdot h(\tau) \cdot \exp(-\lambda) \quad (1)$$

where $C_{\text{out}}(t)$ is the tritium output, $C_{\text{in}}(t-\tau)$ is the tritium input, $h(\tau)$ is the system response function, λ is the radioactive decay constant, t is the time scale and τ is the transit time.

To calculate residence time distributions, the hydrological system has to be conceptualized, which might either follow the piston flow, the completely mixed reservoir or dispersion approach (Małoszewski and Zuber 1982). Assuming that groundwater is being recharged in the catchment area and gets mixed with groundwater in the aquifer, the exponential model was applied to calculate the mean residence time (Eq. 2)

$$h(\tau) = \frac{1}{\tau_0} e^{-\left(\frac{1}{\tau_0}\right)t} \quad (2)$$

where τ_0 is the turnover time of the system. τ_0 is identical to the mean transit time in the uniformly mixed reservoir (Yurtsever 1983). The system response function described by Yurtsever (1983) represents the distribution of the transient time of the tracer input–output function.

^{14}C analysis allows the estimation of groundwater age between 1,000 and 40,000 years (Fritz and Fontes 1980, 1983; Wassenaar et al. 1991) depending on its activity in the total dissolved inorganic carbon (DIC). One sample (1 L) was collected from the main spring S5 at St. Anthony to determine the groundwater age using the ^{14}C technique. Emphasis was placed on the minimization of gas exchange between emerging the groundwater and atmosphere. The almost neutral pH (7.82) (Table 1) was later enhanced to a value of 12 by adding NaOH. Later, CO_2 from the sample is separated by adding phosphoric acid. The ^{14}C activity was subsequently measured using an accelerator mass spectrometry (AMS) at the Hydroisotop Laboratory, Schweitenkirchen (Germany).

The activity ratio of radiocarbon is given in percent modern carbon (pMC) as described in Eq. (3):

$$\text{pMC} = \frac{A_{\text{SN}}}{A_{\text{ON}}} \times 100 \quad (3)$$

where A_{SN} represents the normalized specific activity of the sample; A_{ON} represents the normalized specific activity of oxalic acid (Stuvier and Polach 1977; Mook and van der Pflicht 1999). Groundwater ages (t) are calculated from the general law of radioactive decay and are reported as conventional radiocarbon age in years before present, i.e. before the year 1950 (Geyh 2000; Eq. 4).

$$t = -\frac{1}{\lambda_{\text{C}}} \ln\left(\frac{A}{A_0}\right) \quad (4)$$

A_0 is the initial ^{14}C activity in the recharge, A is the measured activity in the sample, and λ_{C} is the Cambridge decay constant ($\lambda_{\text{C}} = 1/8267$ year^{-1}) which is based on the physical half-life of (5730 ± 30) years. For uncorrected water ages, A/A_0 is equal to $A_{\text{SN}}/A_{\text{ON}}$. To correct the ^{14}C value, ^{13}C (δ^{13}C-DIC) was measured using an isotope ratio mass spectrometer (IRMS) and expressed as permil (‰) referenced to the *Vienna Pee Dee Belemnite* (VPDB) standard: 1 sigma = ± 0.3‰. The sample was analysed in Hydroisotop Laboratory, Schweitenkirchen (Germany).

All determined analyses are presented in Table 1. Since only one floodwater sample could be collected, additional flood water analyses from the El Quseir area (F1) and from El Gouna and Hurghada area (F2–4) were added from literature (Awad et al. 1996).

Hydraulic head measurements in spring S5

Between Nov 2018 and Feb 2019, the discharge and temperature of the major spring S5 in St. Andrews was permanently (30 min interval) recorded applying a temperature and water-table recorder at the artificial tunnel feeding S5.

Remote sensing and GIS-analysis

For the present study, optical, radar and digital elevation data were integrated into the GIS data bank. The satellite data were digitally processed using image processing (ENVI, SNAP) and ArcGIS software. The chosen image processing and RGB-combinations were focused on the enhancement of geologic, tectonic and surface water information. Information on the soil/sediment properties is very important in the scope of these studies as they have an effect on the infiltration capacity of surface water and water storage.

With its 14 spectral bands from the visible to the thermal infrared wavelength region, and its spatial resolution of 15–90 m, ASTER images were included in these investigations, especially the thermal bands. The RGB images created with the bands 10, 12 and 13 were converted from raster into polygon-shapefiles. The lowest values were extracted to get information on potential soil humidity lowering the reflectance in the thermal spectrum. The thermal bands of Landsat 8 were included as well.

Special attention was directed at precise mapping of traces of the tectonic pattern visible on satellite imageries, predominantly on areas with distinct expressed linear features (tonal linear anomalies, geomorphologic linear features, etc.). Lineament analysis helps to reveal traces of the tectonic structure. The term lineament is a neutral term for all linear,

rectilinear or curvi-linear elements. Lineaments are often expressed as scarps, linear valleys, narrow depressions, linear zones of abundant watering, drainage network, and geologic anomalies. Tonal linear anomalies such as the linear arrangement of pixels depicting the same colour/grey tone were visually mapped as linear features as well as lineaments.

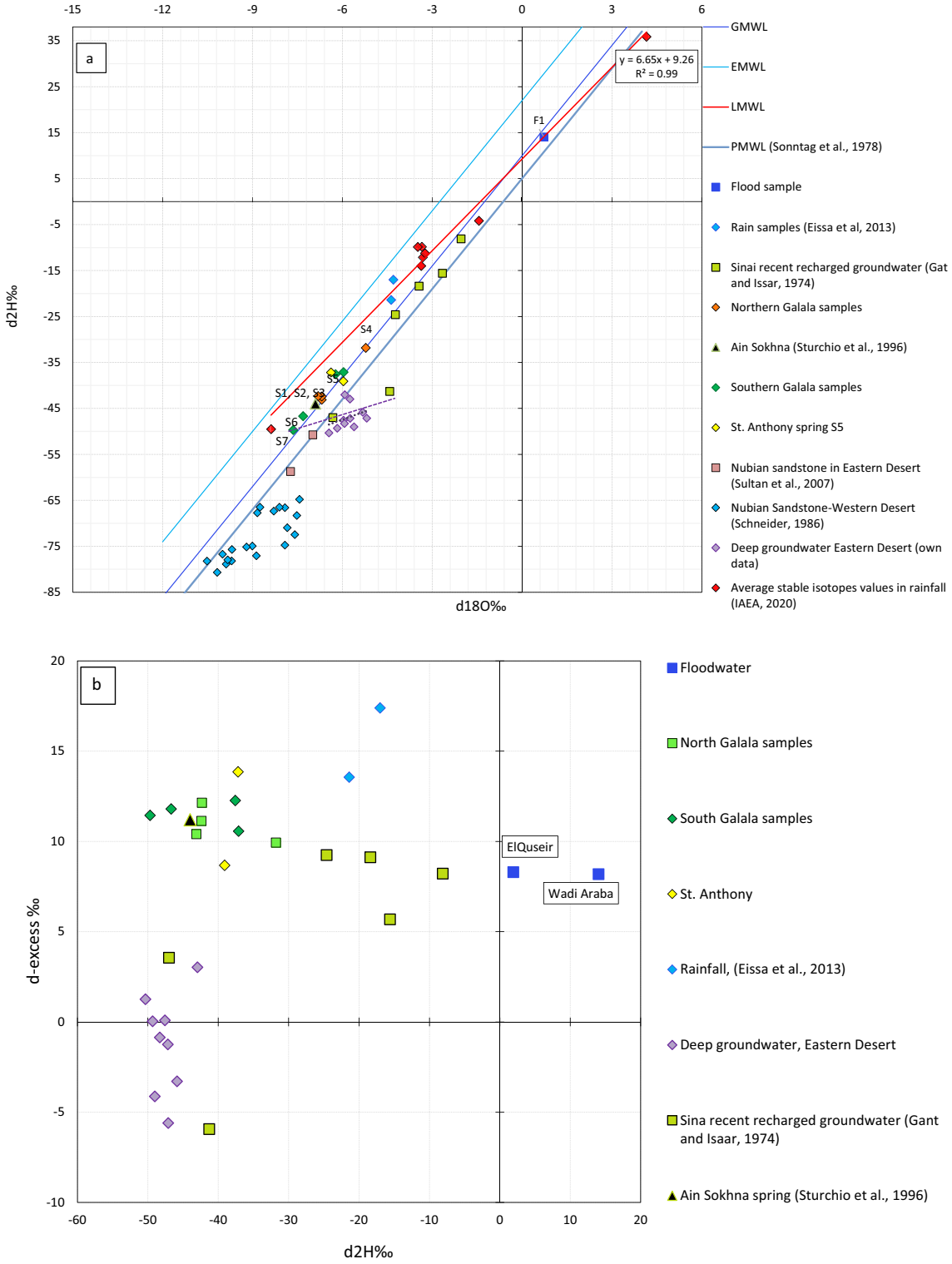

Fig. 8 **a** ^{18}O-^{2}H values in springs of Wadi Araba and their relation to other samples from Eastern Desert (Gat and Issar 1974; Sultan et al. 2007) and Western Desert (Schneider 1986). The Paleo Meteoric Water Line (PMWL) is constructed according to Sonntag et al. (1978). **b** Relationship between d-excess and $\delta^{2}H$ in springs of Wadi Araba and their relation to other samples from Eastern Desert, Sinai Peninsula

Structural features and lithologic units are better visible when merging RGB image products with filter-tool enhanced images. Low-pass and high-pass filters and directional variations were used for the detection of subtle surface structures. Merging the "morphologic" image products derived from "morphologic convolution" image processing in ENVI software with RGB imageries, the structural/tectonic evaluation feasibilities were improved. Surface-water input and resulting infiltration might be influenced by the fault and fracture pattern in the subsurface leading to a relatively higher permeability and hydraulic conductivity.

Results and discussion

Stable isotope content in flood water and groundwater

The floodwater sample F1 lies on the local meteoric water line (LMWL) and the global meteoric water line (GWML; Craig 1961; Fig. 7), indicating no fractionation of the rainfall's signature due to evaporation. Comparing this sample with rainfall samples from the Sinai Peninsula (El Sayed 2006; Eissa et al. 2013) shows that rainfall in Wadi Araba is isotopically heavier than the Sinai rainfall. That might be related to the air mass movement from S to N (NOAA HYSPLIT model using GDAS meteorological data), indicating a rainout of heavier isotopes along the path and depleted signatures in Sinai.

After Dansgaard (1964), the deuterium excess value (*d*) can be determined with $d = \delta^2H - 8\delta^{18}O$. This parameter is strongly dependent on the relative humidity and kinetic effect during evaporation (Merlivat and Jouzel 1979). A d-excess of 8.2‰, as calculated for F1, indicates a relative humidity of about 80–85% (Gonfiantini 1986; Pfahl and Sodemann 2013), preventing significant evaporation prior to or during runoff.

Similar to the floodwater sample F1, groundwater samples (S1–S9) from the springs (with an average value of $\delta^{18}O = -6.55‰$, $\delta^2H = -40.9‰$) lie on the GMWL too. That fact confirms a fast infiltration process where evaporation does not play a role (Fig. 7a), usually provided by fast infiltration into highly permeable sediments or open (karst) conduits, which swallow precipitation immediately.

Groundwater from S6 and S7 show the most depleted $\delta^{18}O$ and δ^2H ratios, revealing either cooler recharge conditions or a higher elevated catchment area. Contrastingly, S4 which is located on the northern flank of Wadi Araba, might be recharged at a lower morphologic position compared to the other springs. Isotope values from S1, S2, and S3 resemble those of the famous Ain Sokhna, which discharges in Suez from the NSAS and is assumed to have been recharged during the late Pleistocene (Sturchio et al. 1996). That similarity may point to the same feeding aquifer and will be discussed in section 'Concentrations of selected major ions and trace elements'.

In contrast to the spring waters, all groundwater from the deep wells in the area of Hurghada, having an average signature of $\delta^{18}O = -5.8‰$ and $\delta^2H = -48‰$, plot well below both the LMWL and GMWL, indicating a systematic evaporation effect. Since the trend line formed by the deep groundwater samples (Fig. 8a) starts from the GMWL close to the isotope ratio of S7, the source of recharge might be similar to S7, but the recharge process is much slower, providing room for evaporation. In that case, the trend line is an evaporation line. Alternatively, the recharge occurs similarly fast as for S7 but mixes later in the subsurface with a second, highly evaporated fluid. In that case, the trend line represents a mixing line. In any case, these deep groundwater samples are more enriched than the samples originating from the Nubian Sandstone in the Western Desert, proven to have been recharged in the Pleistocene era (Sturchio et al. 2004).

Plotting the d-excess of the water against δ^2H (Fig. 8b), two groups of groundwater appear: (1) the deep groundwater with d-excess of <3 and (2) the springs from the Northern and Southern Galala Plateaus with higher d-excess values of >5.

Concentrations of selected major ions and trace elements

Precipitation along the Gulf of Suez is dominated by Cl, SO_4, Na and Ca ions, indicating either the uptake of sea spray or the wash out of halite and sulphate from the atmosphere (Fig. 9a). According to the isotope results, the enhanced mineralization of sampled floodwater (F1) from Wadi Araba, which is 5–15 times higher in salinity than floodwaters from Hurghada and El Quseir, respectively (Fig. 9b), results from interaction of precipitation with the bedrock formations, which collect and transport the runoff. The variability of the Na/Cl ratios in the floodwater in the area of Hurghada (0.82–2.34) indicates different origins, while a value of 0.83 resembles the ratio in seawater, the Na/Cl of 2.34 refers to a different source of Na, probably from weathered plagioclase-rich rock formations (Siebert et al. 2014, 2019). As these formations do not exist in Wadi Araba, the Na/Cl ratio of the floodwater (F1) 0.97 refers to dissolution of halite, which is abundant in the region and has Na/Cl ratio of 1. The enhanced Ca, Mg and SO_4 concentrations in floodwater F1 compared to rainwater are the result of dissolution of gypsum, limestones and dolostones, which are exposed in the Southern Galala Plateau, and the release of these ions during the weathering process. Detectable fluorine (F) concentrations in the Hurghada area indicate release of that element from apatite and fluorite, which occur in the igneous metamorphic rocks of the Red Sea Hills. Since these rocks are missing in Wadi Araba, F is missing in floodwater from Wadi Araba.

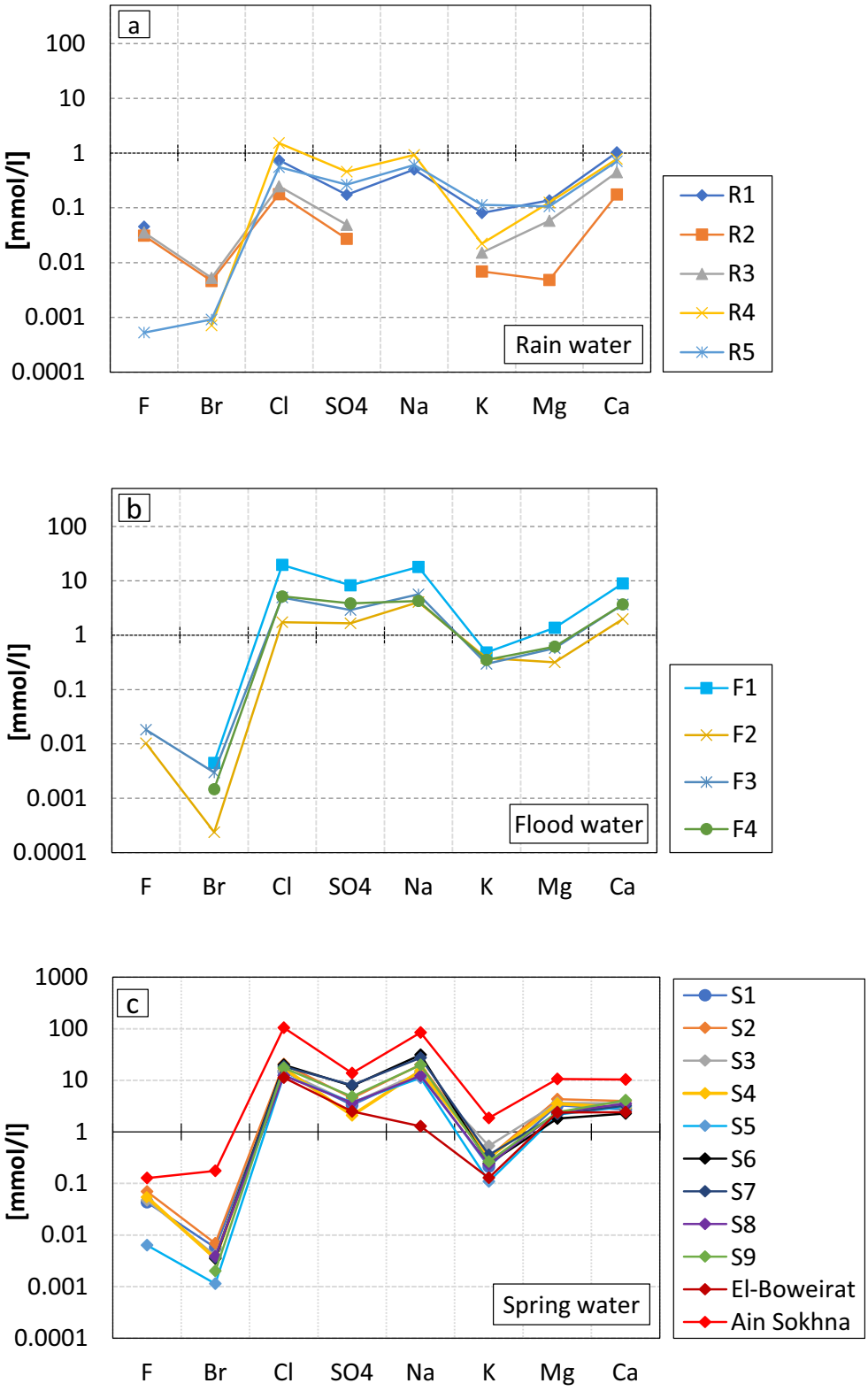

Fig. 9 Schoeller-plots of the hydrochemical analysis of **a** rainfall samples, **b** floodwater samples and **c** groundwater samples. Ain Sokhna sample is derived from Sturchio et al. (1996) and El-Boweirat sample (Central area of Wadi Araba) from Nassim (1990)

To bring spring waters into context to earlier studies, analyses from Ain Sokhna spring (Sturchio et al. 1996) and Ain El-Boweirat (Nassim 1990; Fig. 2, currently dry) were included in Fig. 9c, where spring water composition is given. Groundwater in the southern Galala seem to have lower fluorine concentrations than groundwater from the northern rim.

While Ca and SO_4 content in spring waters is lower than in floodwater, Cl, Na and Mg concentrations in spring waters are

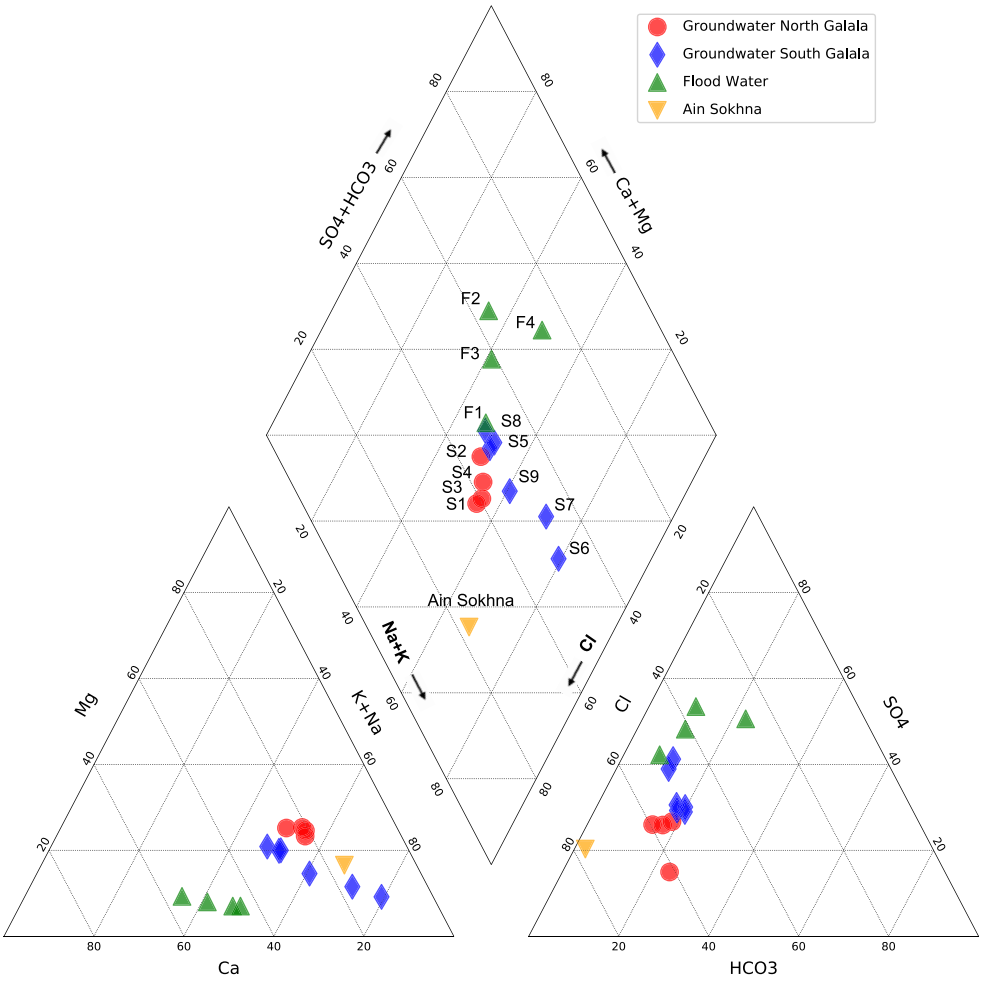

Fig. 10 Piper plot with the compositions of the hydrochemical groups in the investigation area

larger than those of the floodwater F1. That issue refers to the dissolution of aerially imported gypsum by floodwater, while groundwaters dissolve halite and Mg-minerals, which may exist in the local aquifer.

Calculation of molar Ca/Mg ratio shows that groundwater in springs from northern Galala (S1–S4) receive slightly more Mg from aquifer rocks than those from the southern Galala (S5–S9). While the former show low ratios (0.83–0.98) those of the latter range from 1.25 to 1.7, indicating different aquifers of origin. Floodwater ratios are much higher (6.02–6.52), which is the result of additional gypsum, which does not originate locally. Considering SO_4/Cl equivalent ratios, differences are again observable between both spring regions. Groundwater in the northern rim shows ratios of 0.24–0.49, while those in the southern Galala springs are higher (0.56–0.87). Separation is also given comparing Mg/Cl equivalent ratios, which are high in the north (0.41–0.49) and low in the south (0.18–0.41), which indicate a larger content of dolomite in the aquifer feeding the northern springs compared to that supplying the southern group of springs. This is supported by saturation indices (calculated applying PHREEQC Interactive, version 3.3.9 (USGS 2020)). Groundwaters in the north are oversaturated in respect to dolomite, while those in the south are undersaturated.

Concerning the absolute salinity expressed as TDS, all groundwaters are brackish (1,500–2,600 mg/L) and not suitable as potable water. The modified Piper diagram (the position of Cl and $HCO_3 + CO_3$ is switched for a better representation, Fig. 10) shows the hydrochemical characteristics of the spring water.

Groundwater samples S5 and S8 seem to be not influenced by salinities which increase in S9 at St. Paul and continue to increase in S7 and S6. Ain Sokhna is most saline and has a different composition than all other groundwater samples in the northern group, referring to a different aquifer of origin. The dissolution of calcite and dolomite is lowest in groundwaters from S6 and S7, while the alkaline concentrations are highest. Field observations indicate the spring water seems to be partly recharged from the thick rubble overburden, which serves as storage. Though springs at S6 and S7 emerge close to S5 and S8, they emerge from different aquifers. While S5 and S8 originate from fractures and fissures in limestone, S6 and S7 obviously flow out of the shallow unconsolidated

material. Hence, the hydrochemistry between both types of springs differ as stable isotope do.

Groundwater age

Springs with detected ^{3}H

The tritium content detected in the groundwater samples in the area of SAM and SPM are equally low. The detectable concentrations belong to samples S6, S7 and are in a range between 1.1 and 1.5 TU (Table 1).

There are no records for ^{3}H content in precipitation at the Red Sea Coast. The ^{3}H values that were recorded in Alexandria at the Mediterranean Coast are limited to the period 1960–1979 and show a gradual decrease of its concentration, which reached 5.2 TU in 1979. Nevertheless, records from the Bet Dagan station in Israel (31°59′50.29″N, 34°48′58.17″E; IAEA 2020) are available from 1961 till May 2001 with a last recorded value of 5.5 TU. At Ottawa station in Canada (45°19′11.99″N, 75°40′11.99″W; IAEA 2020) the ^{3}H contents record is available till March 2019. The ^{3}H activities in Ottawa station have a constant average value of 13 TU in the period 2013–2018. The assumption that ^{3}H has not changed in the last 5 years together with the measured value of ^{3}H in floodwater (Table 1) enables an estimation of the mean residence time of the groundwater which contains ^{3}H.

Equation (2) was applied to calculate the tritium content curves for different time intervals 0, 5, 10, 15, 20, 25, 30 years for the ^{3}H (average weighted mean value) in the Bet Dagan station (1960–2000). The curves were calculated using a simple calculation model which was developed initially by Yurtsever (1983). The following assumptions were applied:

- For samples from 2000 to 2008, ^{3}H activity was compared with measured values in precipitation in the Bloudan station, 30 km NW of Damascus in Syria (Al Charideh and Abou Zakhem 2010).
- ^{3}H concentrations have not changed in the period 2008–2019 with an average value of 3.8 TU

^{3}H output content in groundwater for the period 1960–2019 was calculated for samples S6, S7 and S9 in the sampling year 2019 after three periods of 5, 10 and 15 years. The calculated residence times which correspond to the measured contents are 15 years for springs S6 and S9, and 10 years for spring S7. Depending on the concentrations of ^{3}H in rainwater, the recent proportion of the water in S6, S7 and S9 could be estimated between as 29% and 39% in the reservoirs that feed these springs.

^{14}C in the main spring S5 of SAM

In sample S5, which came from the permanent spring at SAM, the activity of ^{14}C and the content of ^{13}C in total DIC were determined as 3.86 pMC and −7.8‰, respectively. Depending on the radioactive decay, the age can be determined (Eq. 5; Clark and Fritz 1999).

$$t = -8267 \cdot \ln\left[\frac{a_t \cdot {}^{14}C}{q \cdot a_0 \cdot {}^{14}C}\right] \quad (5)$$

where t is the half time of ^{14}C (5730 ± 30 years), a_0 is the initial activity of ^{14}C, a_t is the measured activity in the sampled water and q is the dilution factor.

Schneider (1986) estimated the initial activity a_0 as 85 pMC when estimating groundwater age from the Nubian Sandstone in the Western Desert of Egypt. This value was adopted for the calculations made here, and leads to an age estimation of 25,690 years which likely represents an overestimate (Buckau et al. 2000).

The concentrations of ions in S5 (Table 1) show that the ionic ratio Ca:Na is 0.56, confirming a contribution of calcite minerals from the aquifer, hence the correction model should consider the dissolved carbonate in the aquifer and consequently the $\delta^{13}C$. Pearson (1965) and Pearson and Hanshaw (1970) defined the dilution factor for the $\delta^{13}C$ correction model (Eq. 6) as:

$$q = \frac{\delta^{13}C_{DIC} - \delta^{13}C_{carb}}{\delta^{13}C_{soil} - \delta^{13}C_{carb}} \quad (6)$$

where $\delta^{13}C_{DIC}$ is the measured ^{13}C in groundwater, $\delta^{13}C_{soil}$ is equal to $\delta^{13}C$ of the soil CO_2 (usually close to −23‰), and $\delta^{13}C_{carb}$ is equal to $\delta^{13}C$ of the calcite being dissolved (usually close to 0‰) (Clark and Fritz 1999). Calculating q results in a dilution factor of 0.3 and t is consequently 15,856 years.

Processing of satellite images

The structural/geologic evaluation of optical satellite images and of radar data allows a reasonably precise mapping of larger lineaments, many of which are probably fault zones (Fig. 11). The evaluation of Landsat 8 and Sentinel 2 based filter images (Fig. 10a), which enhances surface topography, reveals prominent linear and parallel features. In parallel, equidistant linear features become visible on the satellite images processed with directional filters in ENVI in the areas covered by the youngest sediments. These parallel lineaments might reflect the stress pattern of the actual geodynamic activity. The most prominent lineaments are oriented in the NW–SE and NNW–SSE directions. The orientation and occurrence of these prominent linear features on the satellite images are obviously related to the subsurface tectonic pattern,

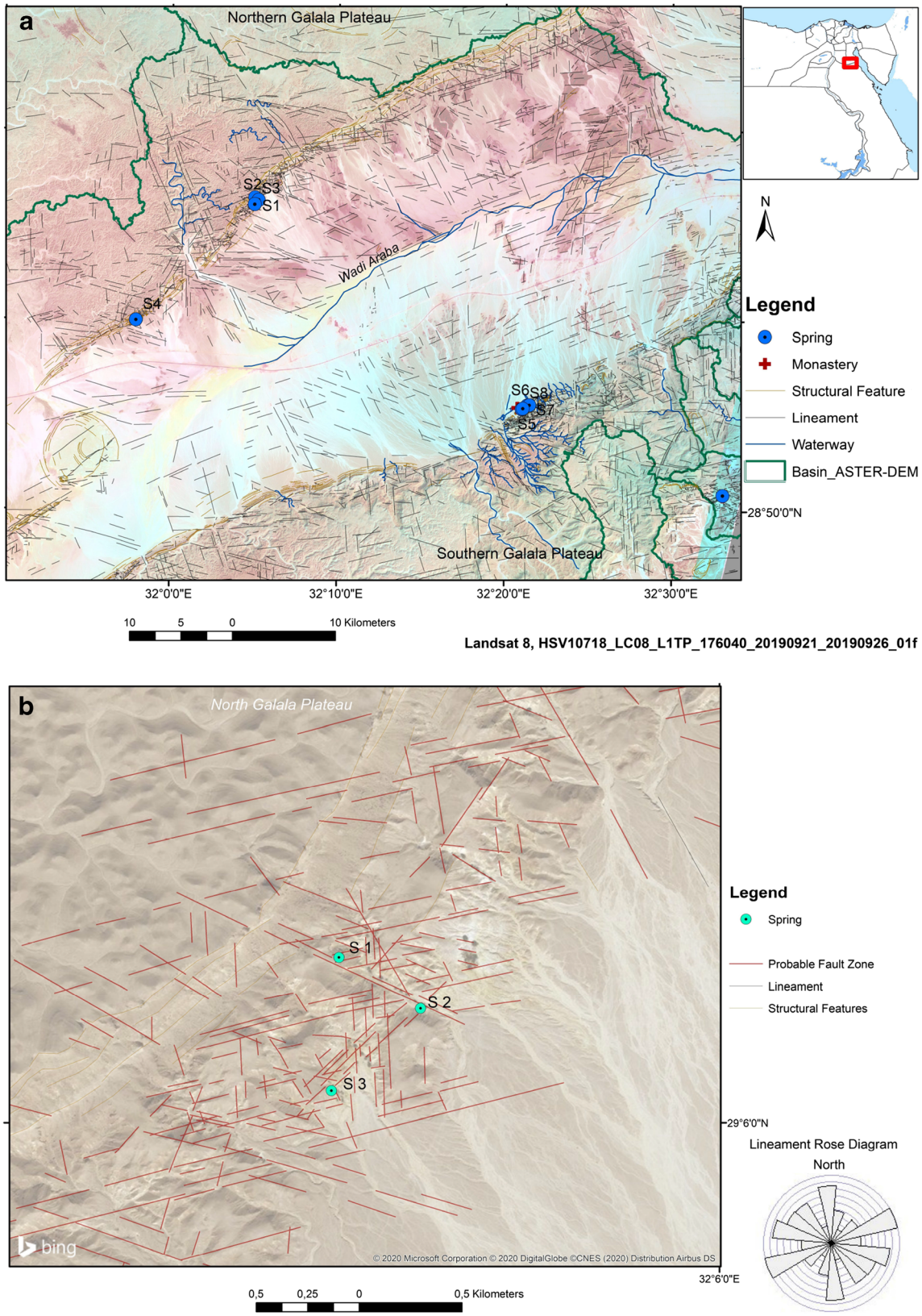

Fig. 11 **a** Lineament map of Wadi Araba and adjacent areas based on Landsat, Sentinel 2, and ASTER satellite data and BingMapsAerial: the rose diagram indicates the direction distribution of lineaments (azimuth-frequency); **b** lineament distribution in the northern escarpment with focus on the spring locations; **c** lineament distribution in the southern escarpment with focus on SAM area. **d** lineament distribution in SPM area

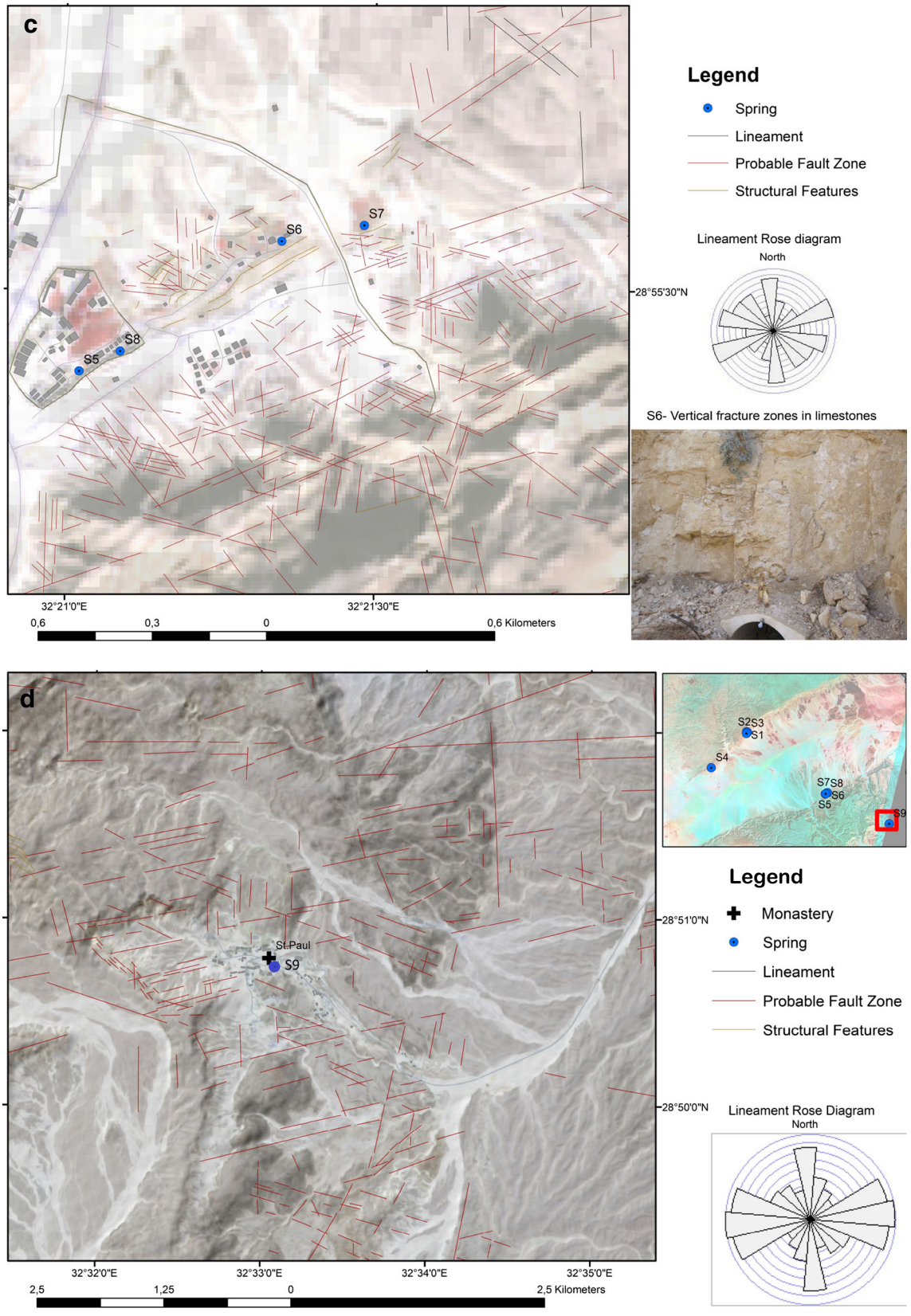

Fig. 11 (continued)

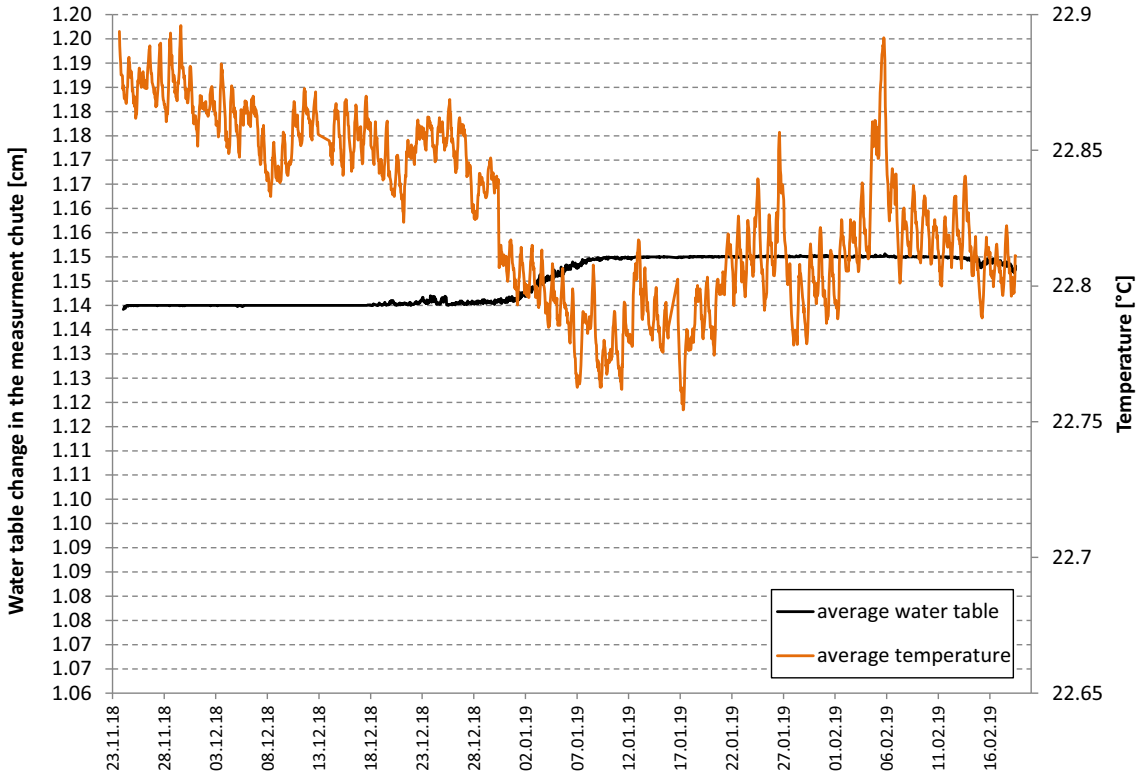

Fig. 12 Hydrograph of the main spring S5 in the period between November 2018 and February 2019

characterized by block faulting (Nassim 1990). Larger fault and fracture zones might have an influence on groundwater flow as indicated in Fig. 11c, showing the example of the area of SAM. Fracture zones are most important for infiltration, migration, and storage of groundwater. The transmissive properties of the dominant rocks in this area are dependent on the presence of fracture zones to provide porosity and permeability. Whenever surface-water infiltrates after precipitation, it is likely that the infiltrated water flow is concentrated along the more permeable fracture zones. In the case of the St. Anthony area, several larger fault zones are intersecting, striking in SW–NE, NW–SE, N–S and NNW–SSE directions. The springs are aligned along the SW–NE-oriented fault zone bordering the Wadi Araba basin in the south.

The lowest and flattest areas are more susceptible to higher surface water flow. During extreme rainfall events in the flatter areass, the run-off concentration is slower and infiltration in sediments and structures is possible. Wadis were developed along weak zones representing fractures or faults; therefore, groundwater recharge may take place in the flat part and the wadis of the Galala Plateaus.

Hydraulic head measurements at the main spring S5 of SAM

Over the period of observation, the hydraulic head in spring S5 oscillated between 1.14 and 1.15 cm. Because of the exchange of air in the cave where the spring occurs, the temperature differences in the measurements reflect the differences of air temperature (Fig. 12).

Discussion

The recent opening of the Gulf of Suez has extended N–S and perpendicular striking fractures in the area of SAM which is evident on the geological map (Fig.5) and on the satellite image (Fig. 11c). The springs S1, S2, S3 and S4 at the Northern Galala Plateau are not permanently flowing and the recharge probably takes place mainly in karst features (Fig. 11b) after rain events. The temperature of the water in the northern samples reflects the mean air temperature (Fig. 4) and is different from the spring water at the Southern Galala Plateau. The residence time seems to be relative short and the ion content is similar to that of the floodwater. The flow of these springs decreases slowly after a stormwater event, and during sampling the water was almost stagnant. Apparently, no reservoirs of the limestone beds can store water for long periods in the system, resulting in a continuous discharge from the springs.

The satellite images and field inspection at the springs of Southern Galala (S5, S6, S7, S8, S9) show evidence of block sliding at the South Galala escarpment (Fig. 11c). Structures are obviously showing the pathway for the groundwater as the springs at St. Anthony emerge from fractures. The geological

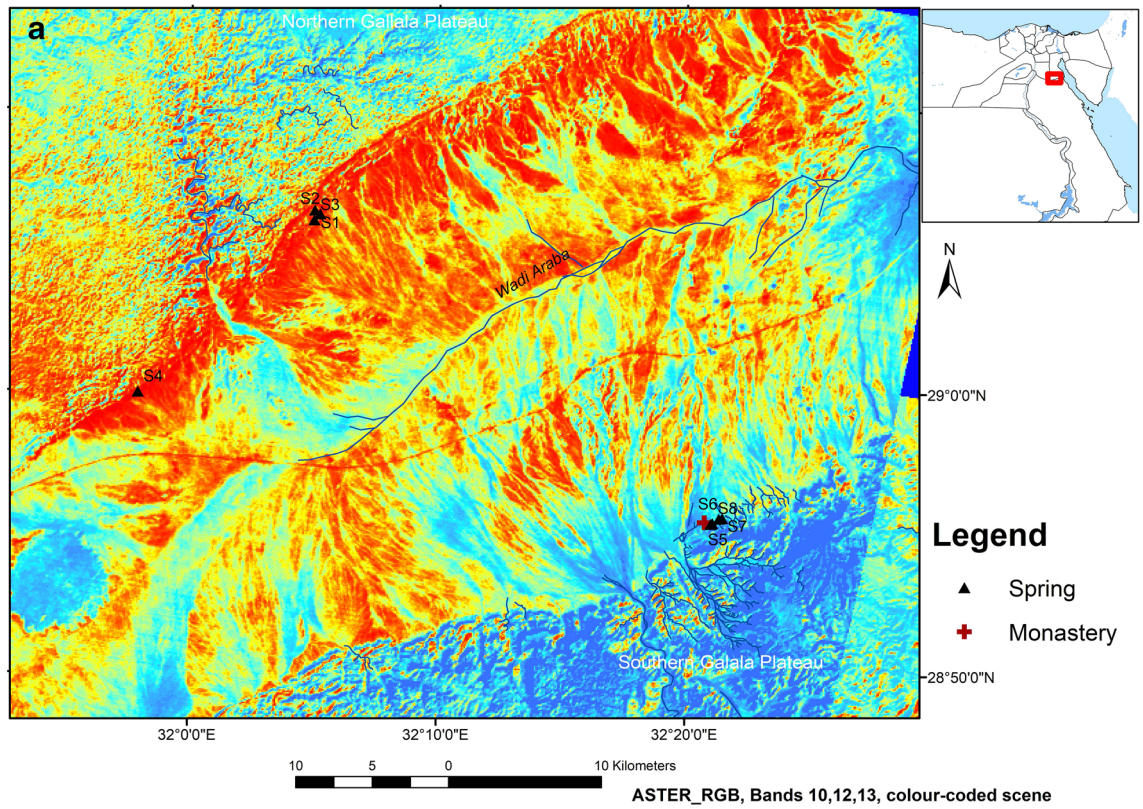

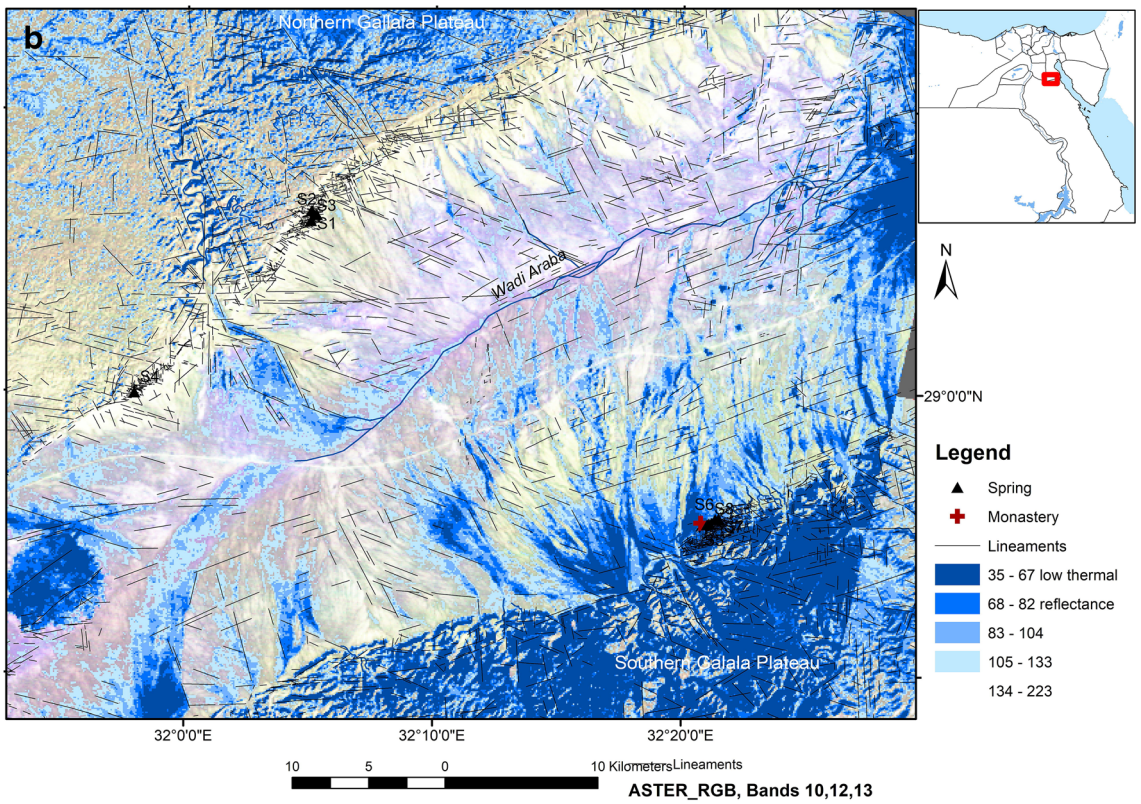

Fig. 13 **a** ASTER scene showing the color-coded thermal bands - ASTER Thermal Bands, RGB: 10, 12, and 13 (acquisition date 14 November 2018), lower thermal reflectance values – blue; **b** extraction of the lower values of the thermal reflectance values based on the ASTER RGB image, indicating areas within the piedmont planes and alluvial fans that might contain relatively higher soil moisture (lower reflectance in the thermal bands)

map (Klitzsch et al. 1987; Fig. 5) together with the geological section of Höntzsch et al. (2011; Fig. 7) confirm that the Southern Galala springs are situated at the ESE–WNW striking Wadi Araba Fault, at the boundary of pre-Campanian marls and Campanian carbonates (Scheibner et al. 2003). Groundwater from the Nubian Sandstone can rise up here because the fault at this site forms a barrier for the groundwater flow. In this context, the age (15,000 years) of S5 water and the absence of ^{3}H in the S8 sample may refer to a partial origin from the Nubian Sandstone aquifer.

The field observations in the area of the SAM and SPM confirm the existence of caves and the cavernous limestone in the escarpment. These caves seem to play the most important role in the regulation of the constant flow of the springs S5 and S8 in St. Anthony. Rainwater from different event intensities infiltrates directly in fractures and fissures at the rim of Galala escarpments. This infiltration process seems to influence the water in springs S6 and S7 where ^{3}H was detected.

The main storage medium of the water for all springs at the southern Galala Plateau must be the karstified limestone of the Maastrichtian age positioned above the thick marls of Campanian age. The water accumulates in huge caves from where the water flows in very tight fractures to the springs. The variation of hydraulic head in the reservoir caverns is very low; thus, the discharge of the springs is relatively constant, as proven by various measurements during the field work. The age of the spring water S5 proves this hypothesis.

Accordingly, two spring groups can be identified on the springs line: S5 and S8 (SW group) in the west, and S6 and S7 (SE group) east of the others. The stable isotope contents are also different in the two groups and the water from the SW group is slightly lighter than that from the SE group. The chemical composition of the SW group is quite different from that of the SE group. The electrical conductivity of the water from the SE group is much higher than that of the SW group but it is the sodium chloride content which makes the difference. In the floodwater from recent rainfall, the sodium chloride content is almost the same as in the SE springs. As no evaporites are shown in the column profiles from Scheibner et al. (2003), and the NaCl content in the water from the SW group is almost half, the sodium chloride content of the SE springs has its origin in recent rainwater. Both springs are located lower at the escarpment than the springs of the SW group and rock rubble lies above and around them. The sulphate content can be explained in the same way. The rainfall seems to discharge the higher salty water at the foot of the escarpment. The easternmost spring (Agathon, S7) occurs at a depth of some meters in an excavation and proves the mixture of young and old (fossil) water. As springs S6 and S7 are located in areas with higher soil moisture (Fig. 13), it is possible to find further springs which might be located in the piedmont planes and alluvial fans that might contain relatively higher soil moisture (Fig. 13b).

Conclusions

In the Galala Plateaus, and including the Wadi Araba, periodical heavy rainfall occurs every 3–5 years, recharging the local and regional aquifers. Unconsolidated wadi sediments in, as well as fissured flat areas on top of the plateaus serve as collectors for parts of these heavy rainfall events.

The analysed floodwater in Wadi Araba indicates no fractionation of the rainfall signature due to evaporation and is isotopically heavier than rainfall from the Sinai Peninsula. This water expresses influence from the halite deposits common in the area. Floodwater from Hurghada area is more influenced by weathered plagioclase-rich rock formations in the Red Sea Hills.

The periodic springs at the Northern Galala Plateau are fed by a densely fractured (or karstified) aquifer without retention potential, which is observable from spring water temperatures and chemical compositions that are similar to that of rainfall on one hand and the fast increase and drop of discharge briefly after rainfall starts and ends, respectively. The springs emerge where lineaments are intersected, indicating a structurally controlled flow-paths regime in the background.

Contrasting the extremely variable discharge of springs at the northern plateau, St. Anthony spring, which discharges on the edge of the Southern Galala Plateau, shows no measurable fluctuations, referring to a large reservoir and an aquifer with large retention. The locations of the springs on the Southern Galala escarpment are characterised with high moisture content. It is very likely that further springs can be found at other high-moisture locations like S8 and S7 which are partially recharged from the flood events.

The area of SPM shows a high density of crossed horizontal and vertical lineaments which seems to play a role in transporting recent recharge to the spring S9. Processing of the satellite images shows that not only structures that are important for pathways of groundwater can be extracted, but also possible near-surface groundwater in the wadis that lead to Wadi Araba, which would have to be explored more closely in the future.

Acknowledgments The Monastery of St. Anthony is gratefully acknowledged for their support during this study. Special thanks are directed to Pater Agathon El Antony from St. Anthony's Monastery and Pater Thomas from St. Paul's Monastery. Many thanks go to José Fabio de Carvalho Haesbaert (Geometric Lda, Caldas Novas, Goias) for his technical support. We also thank Mr. Bollkemper for the chemical analysis and Dr. Schneider from the administration office of ZI Campus El Gouna for supporting this work.

Funding Open Access funding enabled and organized by Projekt DEAL.

References

Abdel Moneim A (2005) Overview of the geomorphological and hydrogeological characteristics of the Eastern Desert of Egypt. Hydrogeol J 13:416–425. https://doi.org/10.1007/s10040-004-0364-y

Abdel-Fattah A, Fnais M, Abdelwahed M, El-Nekhely A, Farid W (2013) Fault orientations in the upper crust beneath an intraplate active zone in northern Egypt. Earth Planet Space 65:739–748. https://doi.org/10.5047/eps.2012.12.005

Abouzied SM, Kaiser MF, Shendi EH, Abdel-Fattah MI (2020) Multi criteria decision support for geothermal resources exploration based on remote sensing, GIS and geophysical techniques along the Gulf of Suez coastal area, Egypt. Geothermica 88:101893

Al Charideh A, Abou Zakhem B (2010) Distribution of tritium and stable isotopes in precipitation in Syria. Hydrol Sci J 55:832–843. https://doi.org/10.1080/02626667.2010.487977

Alsharhan AS (2003) Petroleum geology and potential hydrocarbon plays in the Gulf of Suez Rift Basin, Egypt. AAPG Bull 87:143–180

Askar A (2014) Groundwater chemistry and geology of the unconfined aquifer of the region west of El Gouna – Egypt. MSc Thesis, Technical University of Berlin, ZI Campus ElGouna, Berlin

Awad M, Hamza M, Atwa S, Sallouma M (1996) Isotopic and hydrogeochemical evaluation of groundwater at Qusier-Safaga area, Eastern Desert, Egypt. Environ Geochem Health 18:47–54. https://doi.org/10.1007/BF01771131

Bosworth W, Durocher S (2017) Present-day stress fields of the Gulf of Suez (Egypt) based on exploratory well data: non-uniform regional extension and its relation to inherited structures and local plate motion. J Afr Earth Sci 136:136–147. https://doi.org/10.1016/j.jafrearsci.2017.04.025

Buckau G, Artinger R, Geyer S, Wolf M, Fritz P, Kim J (2000) ^{14}C dating of Gorleben groundwater. Appl Geochem 15:583–597. https://doi.org/10.1016/j.jafrearsci.2017.04.025

Clark I, Fritz P (1999) Environmental isotopes in hydrogeology. Lewis, Ottawa

Craig H (1961) Isotopic variations in meteoric waters. Science 133:1702–1703. https://doi.org/10.1126/science.133.3465.1702

Dansgaard W (1964) Stable isotopes in precipitation. Tellus 16(4):436–468. https://doi.org/10.1111/j.2153-3490.1964.tb00181.x

Eissa M, Thomas J, Pohll G, Hershey R, Dahab K, Dawoud M, ElShiekh A, Gomaa M (2013) Groundwater resource sustainability in the Wadi Watir delta, Gulf of Aqaba, Sinai, Egypt. Hydrogeol J 21:1833–1851. https://doi.org/10.1007/s10040-013-1031-y

El Sayed, M H (2006) Comparative study of water quality of the quaternary aquifer in Wadi Watir basin and its delta, Southeast Sinai, Egypt. Egypt Desert Res 56 (1):17–46

El-Naby A, El-Aal M, Kuss J, Boukhary M, Lashin A (2009) Structural and basin evolution in Miocene time, southwestern Gulf of Suez. Egypt N Jb Geol Pal A 251:331–353. https://doi.org/10.1127/0077-7749/2009/0251-0331

El-Naby A, Ghanem H, Boukhary M, El-Aal M, Lüning S, Kuss J (2010) Sequence-stratigraphic interpretation of structurally controlled deposition: middle Miocene Kareem Formation, southwestern Gulf of Suez, Egypt. GeoArabia 15:129–150

El-Sadek M (1998) Airborne spectrometry and magnetometry of Wadi Araba area, northern Eastern Desert, Egypt. PhD Thesis, Faculty of Science, Ain Shams Univ., Cairo, Egypt

El-Sadek M (2009) Subsurface structural mapping of the area lying between Gabal Elgalala Elqibliya and Elgalala Elbahariya, northern Eastern Desert. Egypt J Geophys Eng 6:111–119. https://doi.org/10.1088/1742-2132/6/2/002

El-Sadek M, Tantawi MA, Salem W (1998) Recharge mechanism and salinization trends of the groundwater resources in Hurghada area, Egypt: environmental isotopic and geochemical approach. El-Minia Sci Bull 11(part 1), March 1998

Fontes J (1983) Dating of groundwater, guidebook on nuclear technique. Technical report series no. 91. IAEA, Vienna

Fritz P, Fontes J (1980) Handbook of environmental isotope geochemistry. Elsevier, Amsterdam

Gat J, Issar A (1974) Desert isotopes hydrology, water sources of the Sinai Desert. Geochim Cosmochim Acta 38(7):1117–1131

Geyh M (2000) An overview of 14C analysis in the study of groundwater. Radiocarbon 42:99–114. https://doi.org/10.1017/S0033822200053078

Geyh M, Bender H, Rajab R, Wagner W (1995) Application of 14C-groundwater dating to non-steady systems, application of tracers in arid zone hydrology (proceedings of the Vienna symposium, August 1994). IAHS Publ. no. 232, IAHS, Wallingford, UK

Gonfiantini (1986) Environmental isotopes in lake studies, the terrestrial environment B. In: Fritz P, Fontes JCh (eds) Environmental isotopes in lake studies, handbook of environmental isotope geochemistry. Elsevier, Amsterdam, pp 113–168

Gupta P, Noone D, Galewsky J, Sweeney C, Bruce VH (2009) Demonstration of high-precision continuous measurements of water vapor isotopologues in laboratory and remote field deployments using wavelength-scanned cavity ring-down spectroscopy (WS-CRDS) technology. Rapid Commun Mass Spectrom 23:2534–2542. https://doi.org/10.1002/rcm.4100

Hadidi A (2016) Wadi Bili: example for Flash Floods in Wadis in the Eastern Desert of Egypt, a structural model for evaluation of the groundwater and the artificial recharge. PhD thesis, Technical University of Berlin, Institute of Applied Geoscience, Berlin

Höntzsch S, Scheibner C, Kuss J, Marzouk AM, Rasser MW (2011) Tectonically driven carbonate ramp evolution at the southern Tethyan shelf: the lower Eocene succession of Galala Mountains, Egypt. Facies 57:51–72. https://doi.org/10.1007/s10347-010-0229-x

IAEA (1990) Environmental isotope data no. 9: world survey of isotope concentration in precipitation (1984–1987). Technical reports series no. 311. IAEA, Vienna

IAEA (1992) Statistical treatment of data on environmental isotopes in precipitation. Technical reports series, vol 331, International Atomic Energy Agency, Vienna

IAEA (2009) Sampling procedures for isotope hydrology. http://www-naweb.iaea.org/napc/ih/documents/other/Sampling%20booklet%20web.pdf. Accessed October 2020

IAEA (2020) Global network of isotopes in precipitation (GNIP). https://www.iaea.org/services/networks/gnip. Accessed December 2020

Klitzsch E, Linke HW (1983) Photogeological interpretation map. Conoco Coral, Cairo

Klitzsch E, List FK, Pöhlmann G (1987) Geological map of Egypt, NH 36 SW. Conoco Coral, The Egyptian General Petroleum Corporation, Beni Suef, Egypt

Kuss J, Scheibner C, Gietl R (2000) Carbonate platform to basin transition along an upper Cretaceous to lower Tertiary Syrian arc uplift, Galala Plateaus, Eastern Desert of Egypt. GeoArabia 5(3):405–426

Lucas L, Unterweger M (2000) Comprehensive review and critical evaluation of the half-life of tritium. J Res Natl Inst Stand Technol 105:541–549. https://doi.org/10.6028/jres.105.043\

Małoszewski P, Zuber A (1982) Determining the turnover time of groundwater systems with the aid of environmental tracers. J Hydrol 57:207–231. https://doi.org/10.1016/0022-1694(82)90147-0

Merlivat L, Jouzel J (1979) Global climatic interpretation of the deuterium-oxygen 18 relationship for precipitation. J Geophys Res 84:5029. https://doi.org/10.1029/JC084iC08p05029

Mook WG, van der Pflicht J (1999) Reporting 14C activities and concentrations. Radiocarbon 41(3):227–239

Moustafa AR, El-Rey AK (1993) Structural characteristics of the Suez Rift margins. Geol Rundsch 82:101–109

Moustafa AR, Khalil MH (1995) Superposed deformation in the northern Suez rift, Egypt: relevance to hydrocarbons exploration. Petrol Geol J 18:245–266

Nassim A (1990) Geological and hydrogeological studies on Wadi Araba Area, north Eastern Desert, Egypt. PhD Thesis, Menoufia University, Al Minufya, Egypt

Pearson FJ (1965) Use of C-13/C-12 ratios to correct radiocarbon ages of material initially diluted by limestone. In: Proceedings of the 6th international conference on radiocarbon and tritium dating, Pullman, WA, June 1965, 357 pp

Pearson FJ, Hanshaw BB (1970) Sources of dissolved carbonate species in groundwater and their effects on carbon-14 dating, isotope hydrology 1970. Proceedings of a symposium Vienna: IAEA and UNESCO, Paris, pp 271–286

Pfahl S, Sodemann H (2013) What controls deuterium excess in global precipitation? Clim Past Discuss 9:4745–4770. https://doi.org/10.5194/cpd-9-4745-2013

Saber M, Abdrabo KI, Habiba OM, Kantoush SA, Sumi T (2020) Impacts of triple factors on flash flood vulnerability in Egypt, urban growth, extreme climate, and mismanagement. Geosci J 10(1). https://doi.org/10.3390/geosciences10010024

Scheibner C, Marzouk AM, Kuss J (2001) Shelf architectures of an isolated late cretaceous carbonate platform margin, Galala Mountains (Eastern Desert, Egypt). Sediment Geol 145:23–43

Scheibner C, Kuss J, Seijer RP (2003) Stratigraphic modelling of carbonate platform-to-basin sediments (Maastrichtian to Paleocene) in the Eastern Desert, Egypt. Palaeogeogr Palaeoclimatol Palaeoecol 200:163–185

Schneider M (1986) Hydrogeologie des Nubischen Aquifersystems am Südrand des Dakhla-Beckens, Südägypten, Nordsudan, band 71 [Hydrogeology of the Nubian aquifer system on the southern edge of the Dakhla basin, southern Egypt, northern Sudan, vol 71]. Berliner Geowissenschaftliche Abhandlung, Reimer, Berlin

Schütz KI (1994) Structures and stratigraphy of the Gulf of Suez, Egypt. In: Landon SM (ed) Interior rift basins. AAPG Mem 59:57–96

Siebert C, Möller P, Geyer S, Kraushaar S, Dulski P, Guttman J, Subah A, Rödiger T (2014) Thermal waters in the Lower Yarmouk Gorge and their relation to surrounding aquifers Chem. Erde-Geochemistry 74:425–441. https://doi.org/10.1016/j.chemer.2014.04.002

Siebert C, Möller P, Magri F, Shalev E, Rosenthal E, Al-Raggad M, Rödiger T (2019) Applying rare earth elements, uranium and 87Sr/86Sr to disentangle structurally forced confluence of regional groundwater resources, the case of the Lower Yarmouk Gorge. Geofluids 2019:6727681. https://doi.org/10.1155/2019/6727681

Sonntag C, Klitzsch E, Löhnert E, Shazly E, Münnich KO, Junghans C, Thorweihe U, Weistroffer K, Swailem F (1978) Paleoclimatic information from deuterium and oxygen-18 in 14C dated, north Saharian groundwaters: groundwater formation in the past. Isotopes Hydrol 1978

Sturchio NC, Arehart GB, Sultan M, Sano Y, Abokamar Y, Sayed M (1996) Composition and origin of thermal waters in the Gulf of Suez area, Egypt. Appl Geochem 11(3):471–479. https://doi.org/10.1016/0883-2927(96)00025-X

Sturchio N, Du X, Purtschert R, Lehmann B, Sultan M, Patterson L, Lu Z, Müller P, Bigler T, Bailey K, O'Connor T, Young L, Lorenzo R, Becker R, El Alfy Z, El Kaliouby B, Dawood Y, Abdallah A (2004) One million year old groundwater in the Sahara revealed by krypton-81 and chlorine-36. Geophys Res Lett 31. https://doi.org/10.1029/2003GL019234

Stuvier M, Polach H (1977) Discussion, reporting of 14C data. Radiocarbon 19(3):355–363. https://doi.org/10.1017/S0033822200003672

Sultan M, Yan E, Sturchio NC, Wagdy A, Abdel Gelil K, Becker R, Manocha N, Milewski A (2007) Natural recharge: a key to sustainable utilization of fossil groundwater. J Hydrol 335(1):25–36. https://doi.org/10.1016/j.jhydrol.2006.10.034

USGS (2020) PHREEQC Interactive, version 3.3.9. https://www.usgs.gov/software/phreeqc-version-3. Accessed 2020

Wassenaar L, Aravena R, Hendry J, Fritz P (1991) Radiocarbon in dissolved organic-carbon, a possible groundwater dating method: case studies from western Canada. Water Resour Res 27:1975–1986

Yurtsever Y (1983) Models for tracer data analysis in: guidebook on nuclear techniques in hydrology. Technical report series no. 91. IAEA, Vienna, pp 381–400